Tectonics®

RESEARCH ARTICLE
10.1029/2021TC006704

Key Points:

- Bedrock geology and thermochronometry suggest the Wallowa and Elkhorn Mountains have distinct topographic histories
- The Elkhorn Mountains began to develop after the Eocene accretion of Siletzia
- Topographic relief in the Wallowa Mountains postdates Miocene eruption of the Columbia River Basalt
- Thermochronometry, Columbia River Basalt, North American Cordillera, Western Idaho Shear Zone

Supporting Information:

Supporting Information may be found in the online version of this article.

Correspondence to:

P. Schoettle-Greene,
schoep@uw.edu

Citation:

Schoettle-Greene, P., Duvall, A. R., & Crowley, P. D. (2022). Multiphase topographic and thermal histories of the Wallowa and Elkhorn Mountains, Blue Mountains Province, Oregon, USA. *Tectonics*, *41*, e2021TC006704. https://doi.org/10.1029/2021TC006704

Received 6 JAN 2021
Accepted 31 JAN 2022

Multiphase Topographic and Thermal Histories of the Wallowa and Elkhorn Mountains, Blue Mountains Province, Oregon, USA

P. Schoettle-Greene[1], A. R. Duvall[1], and P. D. Crowley[2]

[1]Department of Earth and Space Sciences, University of Washington, Seattle, WA, USA, [2]Department of Geology, Amherst College, Amherst, MA, USA

Abstract The Mesozoic and Cenozoic history of Western North America is characterized by terrane accretion, volcanism, and orogenesis. This history complicates the interpretation of paleogeography in northeastern Oregon and adjacent Idaho, where the age of mountainous topography in the Blue Mountains Province is important for validating hypothesized Miocene to present geodynamics. In this study, we analyze the distribution of Columbia River Basalt and low-temperature apatite and zircon (U-Th)/He thermochronometry collected from the Wallowa and Bald Mountain Batholiths to refine regional landscape history. These batholiths underly the Wallowa and Elkhorn Mountains respectively, two of the most prominent mountain ranges within the Blue Mountains Province. We find that low-temperature thermochronometry data from the Bald Mountain and Wallowa Batholiths record distinct thermal histories associated with unroofing and magmatism from the Cretaceous to present. We propose that reheating during intrusion of the Chief Joseph dike swarm led to partial resetting of thermochronometers but did not completely overprint recorded Mesozoic to present thermal histories in the Wallowa Batholith. Using modeled thermal histories and the present-day distribution of Columbia River Basalt, we conclude that the Wallowa and Elkhorn Mountains have distinct topographic histories. We propose that the Elkhorn Mountains began to form in the Eocene and that the Wallowa Mountains are geologically young, forming as a result of relief generation after the Miocene eruption of Columbia River Basalt.

1. Introduction

The Elkhorn and Wallowa Mountains in the Blue Mountains Province of northeastern Oregon exhibit significant relief and elevation in a broad low-relief plateau (Figure 1). These mountain ranges expose pre-Cenozoic units below denuded Eocene-Oligocene volcanic rocks, Miocene Columbia River flood basalts (CRB), and Miocene-present volcanic and sedimentary rocks (Figure 1). The Wallowa Mountains are pervasively intruded by the 16–17 Ma Chief Joseph dike swarm (Figure 1; Morriss et al., 2020), source of the CRB, and have been interpreted as the topographic expression of lithospheric removal coincident with CRB eruption (Hales et al., 2005), or Miocene to present extensional breakup of an orogenic plateau (Kahn et al., 2020). The Elkhorn Mountains were not intruded by the Chief Joseph dikes and, despite having similar peak elevations to the Wallowa Mountains (approximately 2,800 vs. 3000 m), have not been prescribed a geodynamic origin. Both proximity and similarity of prominent topography between the two ranges indicate they may share an uplift history. This, however, is inconsistent with delamination models that propose localized uplift of the Wallowa Mountains (e.g., Darold & Humphreys, 2013; Hales et al., 2005).

Topographic histories are often modeled using low-temperature thermochronometry as a proxy for unroofing (e.g., Ehlers & Farley, 2003), enabling the validation of predictions from geodynamic models (e.g., Schoettle-Greene et al., 2020). In practice, however, it can be difficult to directly correlate the record of landscape development provided by low-temperature thermochronometry with a specific geodynamic scenario. This is particularly the case in regions that have experienced magmatically induced reheating episodes (Murray et al., 2018, 2019). In the Wallowa Mountains, previous studies have found that thermochronometers are sensitive to Miocene Chief Joseph dike-induced reheating (Karlstrom et al., 2019; Reiners, 2005b), complicating application of this technique. Often, the pairing of difficult to interpret thermochronometry data with independent temporal constraints for landscape change such as regional unconformities proves effective at constraining landscape development histories (Brown et al., 2017; Clark et al., 2005; Crowley et al., 2002; Zapata et al., 2019). In the Blue Mountains

10.1029/2021TC006704

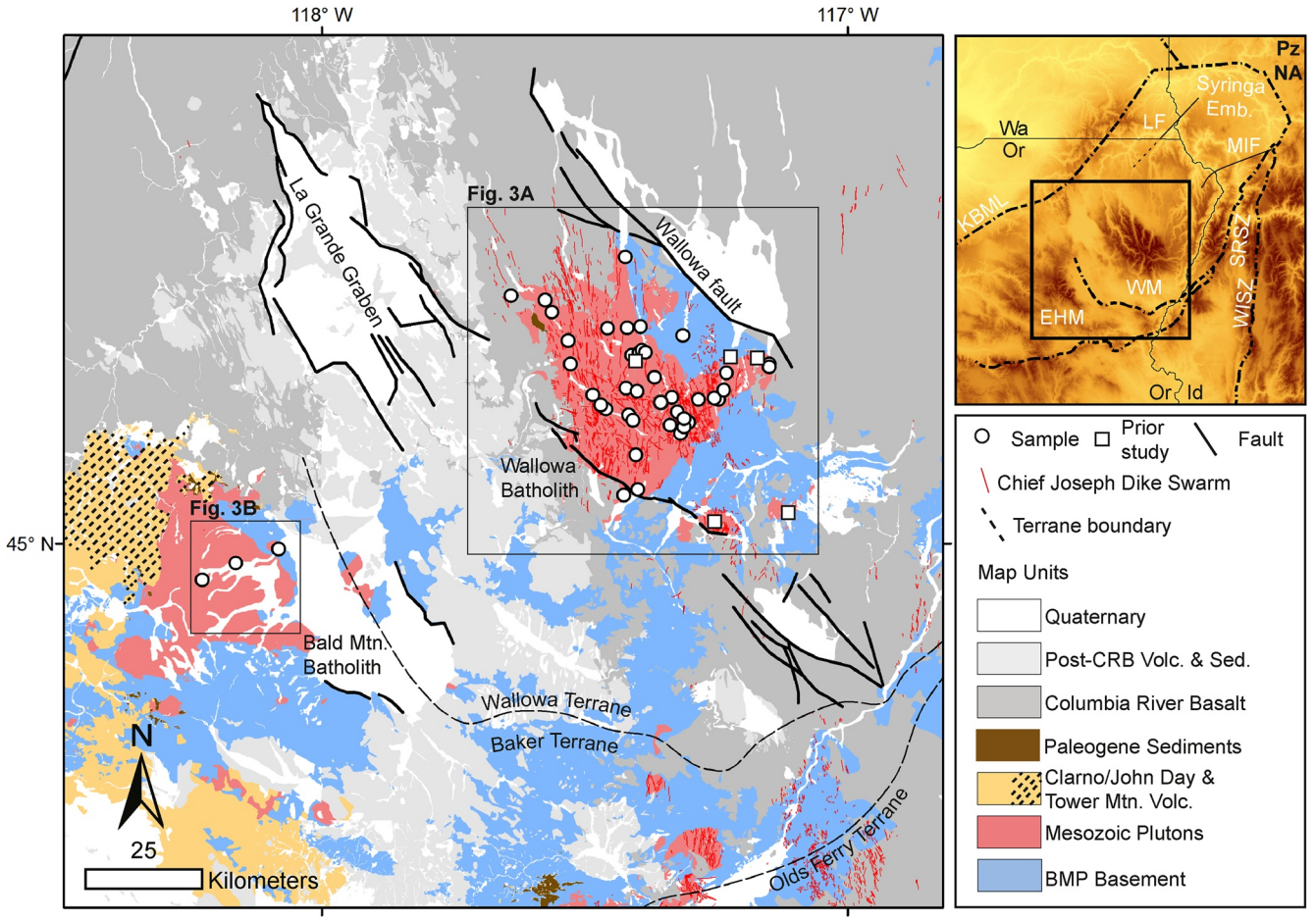

Figure 1. Map of the study area showing surface geology, major faults, sample locations, and terrane boundaries. Inset figure shows regional topography with major lithotectonic terrane boundaries. The Blue Mountains Province encompasses the region between the Klamath-Blue Mountains Lineament (KBML) and the Western Idaho Shear Zone (WISZ) in the inset figure. Chief Joseph dike segments from Morriss et al. (2020). Volcanic units associated with the Tower Mountain caldera marked with hatching. EHM, Elkhorn Mountains; LF, Limekiln Fault; Pz NA, Paleozoic North America; SRSZ, Salmon River Suture Zone; WM, Wallowa Mountains.

Province, Miocene CRB and Eocene-Early Miocene units associated with the Clarno and John Day volcanic province, provide useful datums for exploring changes in Cenozoic topographic relief (Figure 1; Rogers, 1966; Hales et al., 2005).

In this paper, we present new (U-Th)/He dates from the Wallowa and Elkhorn Mountains in the Blue Mountains Province of Oregon and interpret these data in the context of the origins of mountainous topography and the thermal effect of the Chief Joseph dikes. The (U-Th)/He data are paired with regional Cenozoic volcanic stratigraphy to interpret a history of landscape development and tectonics.

1.1. Geologic Background

The Blue Mountains Province comprises volcanic island arc assemblages including the Wallowa and Olds Ferry terranes and a subduction-accretionary prism complex known as the Baker terrane (Figure 1; LaMaskin et al., 2011). The Bald Mountain Batholith intruded the actively deforming suture between the Baker terrane and the Wallowa Terrane from 160 to 140 Ma during and after collision of the Wallowa and Olds Ferry terranes (Schwartz et al., 2010, 2011). Shortly following terrane amalgamation, the Blue Mountains Province collided with North America along the Salmon River Suture Zone. Collision began at 141 Ma and continued to as late as 108 Ma (McKay et al., 2017). During collision, the Wallowa Batholith was intruded from 140 to 120 Ma into the Wallowa Terrane (Figure 1; Žák et al., 2015).

Following accretion, transpression along the right-lateral Western Idaho Shear Zone (WISZ) between 101 and 88 Ma (Braudy et al., 2017; Giorgis et al., 2008), translated the Blue Mountains Province into the Syringa embayment (Figure 1; Schmidt et al., 2017). After translation, the Blue Mountains Province sat inboard of the Farallon/Kula subduction zone during the Laramide orogeny between 90 and 55 Ma. Previous studies suggest that much of the Blue Mountains Province was tectonically quiescent during this period (Gaschnig et al., 2017; Kahn et al., 2020).

In the Cenozoic, the Blue Mountains Province experienced repeated phases of volcanism, beginning with the Eocene Clarno volcanic episode and culminating with eruption of the Miocene CRB. Units associated with the Clarno volcanics are generally found west of the Wallowa and Elkhorn Mountains. Andesitic-dacitic flows and pyroclastics associated with the Oligocene-Early Miocene Tower Mountain caldera and John Day volcanics onlap the Bald Mountain Batholith in the Elkhorn Mountains, locally burying 40–50 Ma boulder conglomerates in contact with batholith rocks (Reiners, 2005a; Ferns et al., 2010). Between 16 and 17 Ma, approximately 163,000 km^3 of the Grande Ronde and Imnaha basalt members of CRB erupted from the Chief Joseph dike swarm in the eastern Blue Mountains Province (Hooper et al., 1984; Kasbohm & Schoene, 2018; Morriss et al., 2020; Reidel et al., 1989), with the greatest mapped concentration of dikes in the Wallowa Mountains (2,300 dike segments, Figure 1; Morriss et al., 2020). CRB buried much of the landscape in the Miocene, locally covering fluvial deposits in the Wallowa Mountains (Allen, 1991), and north of the Elk Horn Mountains (Reiners, 2005a).

Volcanism continued following the CRB with the mid-late Miocene eruption of the Powder River volcanic field on the northwestern flank of the Wallowa Mountains (Figure 1; Ferns & McClaughry, 2013). At the same time, widespread extension in the Blue Mountain Province led to down-dropping of the La Grande Graben starting approximately 9 Ma (Figure 1; VanTassell et al., 2001; Ferns et al., 2010), and reactivation of structures in the Salmon River Suture Zone (Tikoff et al., 2001) and WISZ (Giorgis et al., 2006) as normal faults.

2. Materials and Methods

To determine the tectonic, geomorphic, and thermal evolution of the Wallowa and Elkhorn Mountains, we interpolate a continuous sub-CRB unconformity and analyze new and previously measured (Kahn et al., 2020; Karlstrom et al., 2019) apatite and zircon thermochronometry data from the Wallowa and Bald Mountain Batholiths.

2.1. Interpolation of the Sub-CRB Unconformity

The Imnaha and Grande Ronde members of CRB erupted from the Chief Joseph dike swarm 17 to 16 Ma and flowed across much of the landscape in the study area (Figure 1). Where basalt is preserved, up to 1 km stratigraphic thickness is measured (Camp & Hooper, 1981). The significant thickness of basalt meant that it effectively buried the Miocene landscape and, as a result, preserved evidence of paleo-topography that can be examined today. Furthermore, the degree of post-Miocene deformation and unroofing can be estimated by comparing this paleo-landscape to the present (e.g., Hales et al., 2005; Kahn et al., 2020). Although volcanic units associated with the Oligocene Tower Mountain caldera provide valuable temporal information regarding landscape development in the Elkhorn Mountains (e.g., Ferns et al., 2010), they are not as laterally extensive as CRB, limiting their applicability as a regional datum.

We created a structure contour map of the unconformity between the CRB and older bedrock to estimate the topography of the landscape buried by basalt and provide constraint on the magnitude of burial and post-Miocene exhumation. Using the Oregon state digital geologic map (OGDC-6 2015), as well as regional USGS reconnaissance maps (Swanson et al., 1981), we sampled the elevation of the basal CRB contact with older units. Additional constraint from modeled sub-CRB unconformity depth in Washington (Burns et al., 2011) was used in places with sparse contact exposure. We interpolated a surface through these contacts using the spline with barriers function in ArcGIS v. 10.7. The Wallowa Fault and the fault bounding the southwestern Wallowa Mountains (Figure 1), were included as discontinuities in the interpolation scheme.

2.2. Low-Temperature Thermochronometry

To determine the thermal history of the Wallowa and Elkhorn Mountains region, we analyzed bedrock samples from the Wallowa and Bald Mountain Batholiths using apatite (U-Th)/He and zircon (U-Th)/He methods. Samples

were collected across the Wallowa and Bald Mountain Batholiths and we attempted to avoid sampling close to Chief Joseph dikes. After collection and analysis, sample proximity to mapped dikes was measured using the dike catalog published in Morriss et al. (2020). Below, we briefly review apatite and zircon helium thermochronometry. For a more complete discussion on analytical methods the reader is referred to Supporting Information S1.

2.2.1. Apatite (U-Th)/He Thermochronometry

Apatite (U-Th)/He thermochronometry (AHe) utilizes the temperature dependence of radiogenic helium diffusion in apatite crystals to constrain the timing of cooling from 120 to 30°C (Ault et al., 2019; Flowers et al., 2009; Gautheron et al., 2013). The temperature at which helium is quantitatively retained varies depending on the diffusion kinetics of the apatite crystal which are affected by radiation damage due to alpha ejection (Flowers et al., 2009). Radiation damage is estimated with the proxy eU, where eU = [U] + 0.0235[Th], which predicts a given crystal's potential for damage if held below the crystal lattice annealing temperature. Increasing damage will mean lower helium diffusion rates and a higher closure temperature. Variability in eU has been found to produce substantial date dispersion if samples cool slowly or are reheated after cooling to low temperatures (Ault et al., 2013; Flowers et al., 2007, 2009).

Samples were collected across the Wallowa Mountains at a variety of elevations and on a single transect in the Elkhorn Mountains (Figure 1). Single apatite crystals were selected for analysis based on size, lack of visible inclusions, and euhedral crystal shape. Individual apatite crystals from more recently collected samples (sample prefix WM) were analyzed for U, Th, Sm, and He content at the Caltech Noble Gas Lab. Legacy AHe data (sample prefix WB) used aliquots of 1–5 apatite grains from each sample and were analyzed in 2001 at Washington State University.

2.2.2. Zircon (U-Th)/He Thermochronometry

Zircon (U-Th)/He thermochronology (ZHe) uses the temperature-dependent retentivity of He in zircon crystals to constrain the timing of crystal cooling from 220 to 140°C (Guenthner et al., 2013). Radiation damage also plays a role in determining the temperature at which He is quantitatively retained within a zircon crystal. For zircon, radiation damage may reduce helium diffusivity, increasing the effective closure temperature. Given sufficient damage, however, helium diffusivity increases, decreasing the effective closure temperature (Guenthner et al., 2013). ZHe data used aliquots of 1–5 apatite grains from each sample and were analyzed in 2001 at Washington State University.

2.3. Thermal Modeling of Thermochronometry Data

To better understand the thermal history recorded by thermochronometry data, we used the software QTQt to estimate viable time-temperature histories for the Wallowa and Bald Mountain Batholiths. QTQt uses a Bayesian Monte-Carlo Markov chain method to invert thermochronometry data for viable time-temperature histories (Gallagher, 2012). This technique estimates thermal histories by satisfying constraints provided by individual apatite and zircon crystals as well as user-specified temperature histories. We ran models of individual samples as well as suites of samples that were assumed to share a common cooling history.

For all models, we ran 50,000 burn-in and 10,000 post burn-in steps. Proposals outside the prior were rejected and inversions rejected more complex models that did not improve data fit. All samples use the RDAAM diffusion model for apatite (Flowers et al., 2009) and ZRDAAM for zircon (Guenthner et al., 2013). Errors on all helium dates were assumed to be 10% of the reported date to account for both uncertainty in grain size measurements as well as analytical uncertainty in measured isotope concentrations. A temperature constraint of 900°C was applied at the emplacement date for each pluton. For models that included more than one sample, the acceptable geothermal gradient was limited to 30 ± 30°C/km and allowed to vary over time. The present-day elevation difference or depth below the sub-CRB unconformity between samples modeled in tandem was used to guide estimation of this gradient. In models that included multiple samples, present-day temperature for the highest sample was constrained to 5 ± 5°C, with a terrestrial lapse rate of 3.4°C/km (Salmon River, Idaho; Wolfe, 1992), resulting in a maximum modeled temperature for the lowest sample of approximately 15°C. Additional modeling inputs can be found in Text S1 in Supporting Information S1.

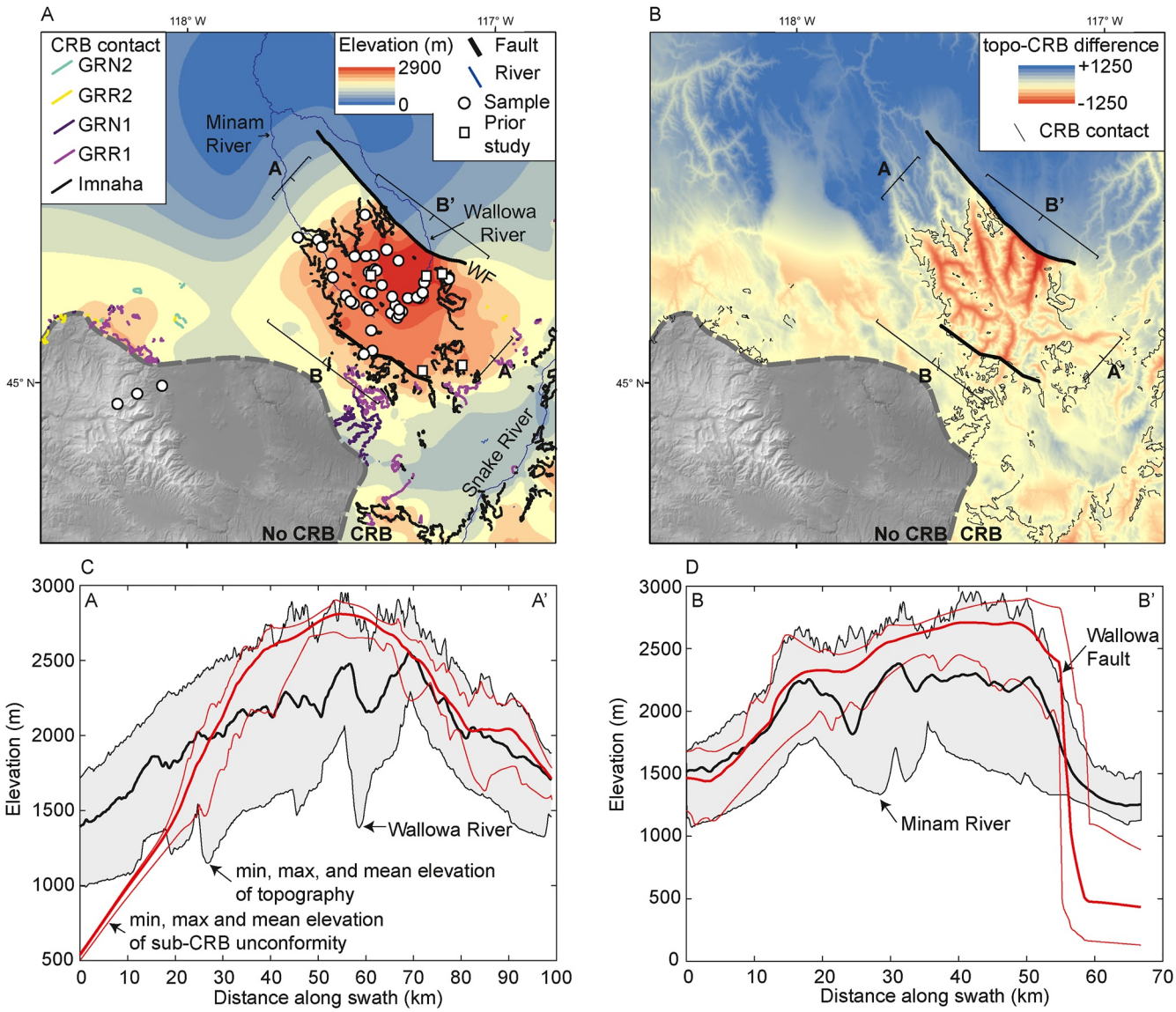

Figure 2. (a) Interpolated sub-CRB unconformity surface with overlain locations of the mapped sub-CRB unconformity contacts, and fault barriers used in surface interpolation. Wallowa and Minam river valleys, which run parallel to swaths A–A′ and B–B′ respectively, are labeled to aid in swath interpretation. GRR1 = Grande Ronde R1, GRN1 = Grande Ronde N1, GRR2 = Grande Ronde R2, GRN2 = Grande Ronde N2. (b) Difference in elevation between interpolated sub-CRB unconformity and present-day topography. (c) Swath profile A–A′ showing present-day topography and the sub-CRB unconformity parallel to the Wallowa Fault. (d) Swath profile B–B′ showing present-day topography and the sub-CRB unconformity parallel to the Wallowa Fault.

3. Results

3.1. Interpolation of the Sub-CRB Unconformity

The interpolated sub-CRB unconformity in northeastern Oregon ranges from 0 to 2,900 m elevation (Figure 2a). No Imnaha or Grande Ronde basalt are mapped southwest of the Wallowa Mountains, thus the interpolation is unconstrained (Figure 2a). In the Wallowa Mountains, where CRB is found on many mountain summits, the sub-CRB unconformity is dome-like in map view and mostly defined by Imnaha basalt (Figure 2a), the oldest CRB unit locally preserved. Across the central Wallowa Mountains, the splined surface is less well constrained, and can be greater than 5 km from the nearest mapped sub-CRB unconformity (Figure S1 in Supporting Information S1). Together with the frequent observation of fluvial deposits beneath CRB (Allen, 1991), indicating preferential preservation of Miocene valley bottoms, the less well constrained portions of the interpolated sub-CRB unconformity across the central Wallowa Mountains should be interpreted as a minimum elevation. This lack of

resolution on the sub-CRB unconformity interpolation limits our ability to determine local paleo-relief within the central Wallowa Mountains.

Regionally, local relief on the surface is minimal and lows are found in the Snake and Grande Ronde river valleys. Greatest local relief on the surface is observed across the Wallowa Fault, where the unconformity drops >2 km. Generally, the southwestern limit of CRB is defined by contacts between Grande Ronde R1 and younger members. Downslope on the southwest flank of the Wallowa Mountains, progressively younger Imnaha and Grande Ronde CRB units are found in contact with underlying pre-Miocene bedrock (Figure 2a).

The difference between the interpolated sub-CRB unconformity and present-day topography is most pronounced in the Wallowa Mountains and to the north (Figure 2b). Elsewhere, the sub-CRB unconformity is interpolated to be within a few hundred meters of present-day topography. North of the Wallowa Mountains, the sub-CRB unconformity is beneath present-day topography. In the Wallowa Mountains, present-day topography is as much as 1,250 m lower than the interpolated sub-CRB unconformity. Generally, valleys on the eastern flank of the Wallowa Mountains do not have present-day elevations that deviate far from the sub-CRB unconformity. In the Wallowa River valley, whose outlet is controlled by the Wallowa Fault, the lowest present-day elevation relative to the sub-CRB unconformity is observed.

Swath profiles over the Wallowa Mountains show the sub-CRB unconformity and present-day topography generally paralleling each other in a broad upwarp across the range (Figures 2c and 2d). A swath drawn parallel to the Wallowa fault shows a maximum approximately 700 m local relief in the unconformity surface and >1 km local relief in present-day topography. Net relief is similar (>2 km) for the sub-CRB unconformity and present-day topography. A profile across the Wallowa Mountains shows both the interpolated unconformity and present-day topography having a block-like form (Figure 2d).

CRB is thickest on the northwestern flank of the Wallowa Mountains, where basalt thicknesses of approximately 800 m are exposed in the Minam and Lostine valleys (Figure 2c). This contrasts with the other flanks of the Wallowa Mountains, where the unconformity surface and present topography are roughly coincident and minimal basalt thickness is preserved (Figure 2c, d). The dips of individual CRB flows are parallel to the dips of the interpolated sub-CRB unconformity on the northwest flank of the Wallowa Mountains and nominally steeper than the sub-CRB unconformity on the southeast flank.

3.2. Low-Temperature Thermochronometry

We present 144 previously unpublished low-temperature thermochronometry AHe and ZHe dates from the Wallowa and Bald Mountain Batholiths (Tables 1, S1, S2 in Supporting Information S1). These include AHe data for 98 individual apatites from 20 bedrock samples collected from the Wallowa and Bald Mountain batholiths of eastern Oregon (Table S1 in Supporting Information S1), 39 legacy AHe dates calculated from aliquots of 1–5 grains from 24 bedrock samples (Table S1 in Supporting Information S1), and 7 legacy ZHe dates calculated from aliquots of 1–5 grains from 7 bedrock samples in the Wallowa Batholith (Table S2 in Supporting Information S1). We further include in our analysis 4 AHe dates from samples 01CS15aB and 2e9 previously published by Karlstrom et al. (2019), and 12 AHe dates from samples Z14BT2, Z14BT3, Z14BT4, and 15MK08 previously published by Kahn et al. (2020). ZHe data are supplemented by one previously published ZHe date from sample Se9 from Karlstrom et al. (2019), and nine dates from samples Z14BT2, Z14BT3, and Z14BT4 previously published by Kahn et al. (2020). The four major plutons of the Wallowa Batholith are well sampled by these data whereas data from the Bald Mountain Batholith are from a single transect up the eastern face of the Elkhorn Mountains (Figure 3).

AHe dates range from 12 to 129 Ma (Table S1 in Supporting Information S1), and ZHe dates range from 20 to 133 Ma (Table S3 in Supporting Information S1). AHe dates from the central Wallowa Batholith are generally youngest, with older dates on the northwestern and southeastern flanks (Figure 3a). ZHe dates are similar across the Wallowa Batholith. In the Bald Mountain Batholith, WM08, the eastern-most and lowest elevation sample, has the oldest AHe date while the two higher elevation samples have similar AHe dates (Figure 3b).

AHe data from the Wallowa Batholith are bimodally distributed with a sharp peak between 10 and 20 Ma and a more diffuse distribution between 60 and 110 Ma, with few dates between 20 and 60 Myr (Figure 3c). In contrast, the majority of AHe dates from the Bald Mountain Batholith are between 30 and 60 Myr, with three dates in the

Table 1
Summary Information for Bedrock Thermochronometry Samples Used in This Study

Sample	Lithology	Longitude (E)	Latitude (N)	# of apatite analyzed[a]	# of zircon analyzed[a]	Elev. (m)	Depth (m)	Avg. AHe corr. date (Ma)	1s (Ma)	AHe date disp. (Ma) 1s/ Avg.	Avg. ZHe corr. date (Ma)	1s (Ma)	ZHe date disp. (Ma) 1s/ Avg.
WM06	Bald Mt Batholith	−118.2280	44.9510	5	-	2499	-	46.08	9.67	0.21	-	-	-
WM07	Bald Mt Batholith	−118.1640	44.9740	5	-	1802	-	49.32	10.47	0.21	-	-	-
WM08	Bald Mt Batholith	−118.0830	44.9930	5	-	1153	-	77.55	25.87	0.33	-	-	-
WM21	Craig Mountain pluton	−117.1500	45.2424	5	-	2162	−82	22.80	4.40	0.19	-	-	-
WM22	Hurricane Divide pluton	−117.4110	45.2545	5	-	2360	−277	94.70	4.43	0.05	-	-	-
WM23	Hurricane Divide pluton	−117.3970	45.2578	5	-	2135	−562	95.10	4.03	0.04	-	-	-
WM24	Hurricane Divide pluton	−117.3910	45.2611	5	-	1860	−901	92.80	6.08	0.07	-	-	-
WM25	Hurricane Divide pluton	−117.3850	45.2581	5	-	1671	−1004	17.10	0.39	0.02	-	-	-
WM27	Hurricane Divide pluton	−117.4600	45.1817	5	-	1567	−743	69.20	4.71	0.07	-	-	-
WM28	Craig Mountain pluton	−117.3920	45.1510	5	-	1644	−767	52.49	14.68	0.28	-	-	-
WM29	Hurricane Divide pluton	−117.4220	45.2100	5	-	2641	−16	94.90	11.10	0.12	-	-	-
WM30	Hurricane Divide pluton	−117.4010	45.2061	5	-	2315	−373	87.30	4.89	0.06	-	-	-
WM31	Craig Mountain pluton	−117.3029	45.1642	5	-	2874	190	18.10	1.13	0.06	-	-	-
WM35	Craig Mountain pluton	−117.3380	45.1599	4	-	2050	−531	86.90	4.39	0.05	-	-	-
WM39	Craig Mountain pluton	−117.2460	45.1947	5	-	1838	−901	16.40	0.41	0.03	-	-	-
WM42	Hurricane Divide pluton	−117.3680	45.2247	5	-	1965	−671	98.10	6.34	0.06	-	-	-
WM51	Needle Point pluton	−117.3990	45.0735	5	-	1549	−731	71.20	5.04	0.07	-	-	-
WM52	Needle Point pluton	−117.4260	45.0660	4	-	1644	−325	83.90	1.97	0.02	-	-	-
WM53	Hurricane Divide pluton	−117.3140	45.2807	4	-	1898	−916	82.50	16.10	0.20	-	-	-
WM54	Hurricane Divide pluton	−117.3340	45.3130	5	-	2332	−304	119.85	10.58	0.09	-	-	-
WB005	Craig Mountain pluton	−117.2310	45.2308	1A	-	1998	−809	70.30	0.70	-	-	-	-
WB009	Craig Mountain pluton	−117.1500	45.2384	2A	-	2188	−39	30.35	0.92	0.03	-	-	-
WB010	Pole Bridge pluton	−117.4230	45.3862	1A	-	1285	−426	83.10	1.00	-	-	-	-
WB017	Pole Bridge pluton	−117.3940	45.2931	1A	-	1608	−1033	106.40	1.20	-	-	-	-
WB034	Pole Bridge pluton	−117.6410	45.3341	1A	1A	1227	−6	15.30	0.10	-	62.6	0.60	-
WB101	Pole Bridge pluton	−117.5760	45.3287	3A	1A	1277	−334	101.87	1.72	0.02	133.4	1.30	-
WB104	Pole Bridge pluton	−117.5630	45.3120	2A	1A	1243	−645	15.80	1.13	0.07	21.4	0.10	-
WB109	Pole Bridge pluton	−117.5320	45.2740	2A	-	1333	−936	86.95	6.29		-	-	-
WB112	Pole Bridge pluton	−117.5280	45.2426	1A	-	1363	−786	38.40	0.50	-	-	-	-
WB118	Hurricane Divide pluton	−117.4850	45.2006	2A	1A	1471	−630	17.40	0.28	0.02	113.1	1.10	-
WB121	Hurricane Divide pluton	−117.4700	45.1876	2A	-	1507	−666	50.95	3.04	0.06	-	-	-
WB130	Craig Mountain pluton	−117.4170	45.1738	1A	1A	1765	−691	77.80	0.70	-	105.5	1.00	-
WB131	Craig Mountain pluton	−117.4090	45.1669	1A	-	1698	−702	72.50	0.80	-	-	-	-
WB139	Needle Point pluton	−117.4030	45.1203	2A	-	1896	−472	76.40	0.57	0.01	-	-	-
WB141	Craig Mountain pluton	−117.3180	45.1490	2A	-	2110	−501	66.75	4.60	0.07	-	-	-
WB143	Craig Mountain pluton	−117.3120	45.1576	1A	-	2240	−373	85.10	0.90	-	-	-	-
WB146	Craig Mountain pluton	−117.3240	45.1780	1A	-	2400	−281	41.80	0.40	-	-	-	-
WB149	Craig Mountain pluton	−117.3120	45.1688	2A	1A	2609	−1	18.20	0.28	-	100.3	1.00	-
WB152	Craig Mountain pluton	−117.2840	45.1948	2A	1A	2248	−514	86.80	1.56	-	105.3	1.00	-
WB154	Craig Mountain pluton	−117.2540	45.1969	1A	-	2014	−600	76.30	0.80	-	-	-	-

Table 1
Continued

Sample	Lithology	Longitude (E)	Latitude (N)	# of apatite analyzed[a]	# of zircon analyzed[a]	Elev. (m)	Depth (m)	Avg. AHe corr. date (Ma)	1s (Ma)	AHe date disp. (Ma) 1s/ Avg.	Avg. ZHe corr. date (Ma)	1s (Ma)	ZHe date disp. (Ma) 1s/ Avg.
WB158	Craig Mountain pluton	−117.2360	45.2076	2A	-	1822	−838	61.10	1.41	0.02	-	-	-
WB166	Pole Bridge pluton	−117.4200	45.2912	1A	-	2252	−401	104.90	0.90	-	-	-	-
WB250	Pole Bridge pluton	−117.4570	45.2906	2A	-	2352	−194	102.10	1.70	0.02	-	-	-
WB267	Craig Mountain pluton	−117.3340	45.1979	3A	-	2159	−525	75.30	4.36	0.06	-	-	-
Z14BT2[b]	Craig Mountain pluton	−117.1756	45.2546	3	3	2474	−20	75.6	3.1	0.04	100.9	9.40	0.09
Z14BT3[b]	Craig Mountain pluton	−117.1780	45.2568	3	3	2457	−85	21.8	10	0.46	112	11.81	0.11
Z14BT4[b]	Craig Mountain pluton	−117.2255	45.2420	3	3	1601	−1151	15.5	0.1	0.01	59.6	21.20	0.36
15MK08[b]	Needle Point pluton	−117.1039	45.0389	3	-	2135	10	93.6	10	0.11	-	-	-
01CS15aB[c]	Needle Point pluton	−117.2500	45.0305	1	1	2238	3	104.6	6.3	-	107.3	6.40	-
2e9[c]	Hurricane Divide pluton	−117.4071	45.2508	3	-	2367	−258	45	4.4	0.10	-	-	-

[a]A = multigrain aliquot. [b]Kahn et al. (2020). [c]Karlstrom et al. (2019).

80 to 100 Ma range (Figure 3c). The majority of ZHe dates in the Wallowa Batholith are between 90 and 130 Ma (Figure 3d). All ZHe dates less than 90 Ma are from samples with AHe dates approximately 17 Ma.

3.2.1. Radiation Damage

Apatites and zircons from the Wallowa and Bald Mountain Batholiths have eU values from 5 to 273 and 53 to 603 ppm, respectively (Figure 4; Tables S1 and S2 in Supporting Information S1). This eU variability is large enough to have a significant impact on AHe and ZHe closure temperature (e.g., Flowers et al., 2009; Guenthner et al., 2013) especially for the AHe system where measured eU covers the published range of naturally occurring eU values. ZHe eU values have a more limited range relative to other data sets (e.g., 270–7200 ppm; Orme et al., 2016), with all but one measured eU value below 400 ppm.

AHe data show a positive log-normal age-eU relationship for dates >20 Ma (Figure 4a), consistent with an eU influence on AHe closure temperature (Flowers et al., 2009; Shuster & Farley, 2009). This trend is most recognizable in samples where individual grains were analyzed and to a lesser degree where multigrain aliquots were used (Figure 4a; Table 1). Wallowa Batholith AHe ages at eU values less than 100–150 ppm are widely distributed, suggesting a complex low-temperature thermal history. Twenty-seven AHe dates between 10 and 20 Ma and with eU values between 5 and 119 ppm show no age-eU relationship (Figure 4a). Bald Mountain Batholith AHe dates show a trend toward increasing age with eU and generally plot in a eU-date region with few Wallowa Batholith dates.

The four Wallowa Batholith plutons sampled in this study show distinct AHe eU values (Figure 4a). Average AHe eU values are 53 ± 16 ppm for the Pole Bridge Pluton, 106 ± 69 ppm for the Hurricane Divide Pluton, 24 ± 12 ppm for the Craig Mountain Pluton, and 67 ± 45 ppm for the Needle Point Pluton. Samples from the Bald Mountain Batholith have eU values ranging from approximately 15 to 111 ppm (Figure 4a).

A paucity of AHe replicates prevents a thorough examination of age-eU trends for samples individually. However, for the 21 samples with more than two replicates, AHe dates tend to reproduce well. Only sample WM08 from the Bald Mountain Batholith shows a strong correlation between eU and date (Figure 4, dashed bold black border), suggesting the wide AHe date dispersion for this sample is not spurious. In contrast, sample WM28, with a bimodal date distribution, does not show an age-eU correlation (Figure 4, solid bold black border). Because we cannot explain the range of AHe dates for this sample, we exclude it from further analysis.

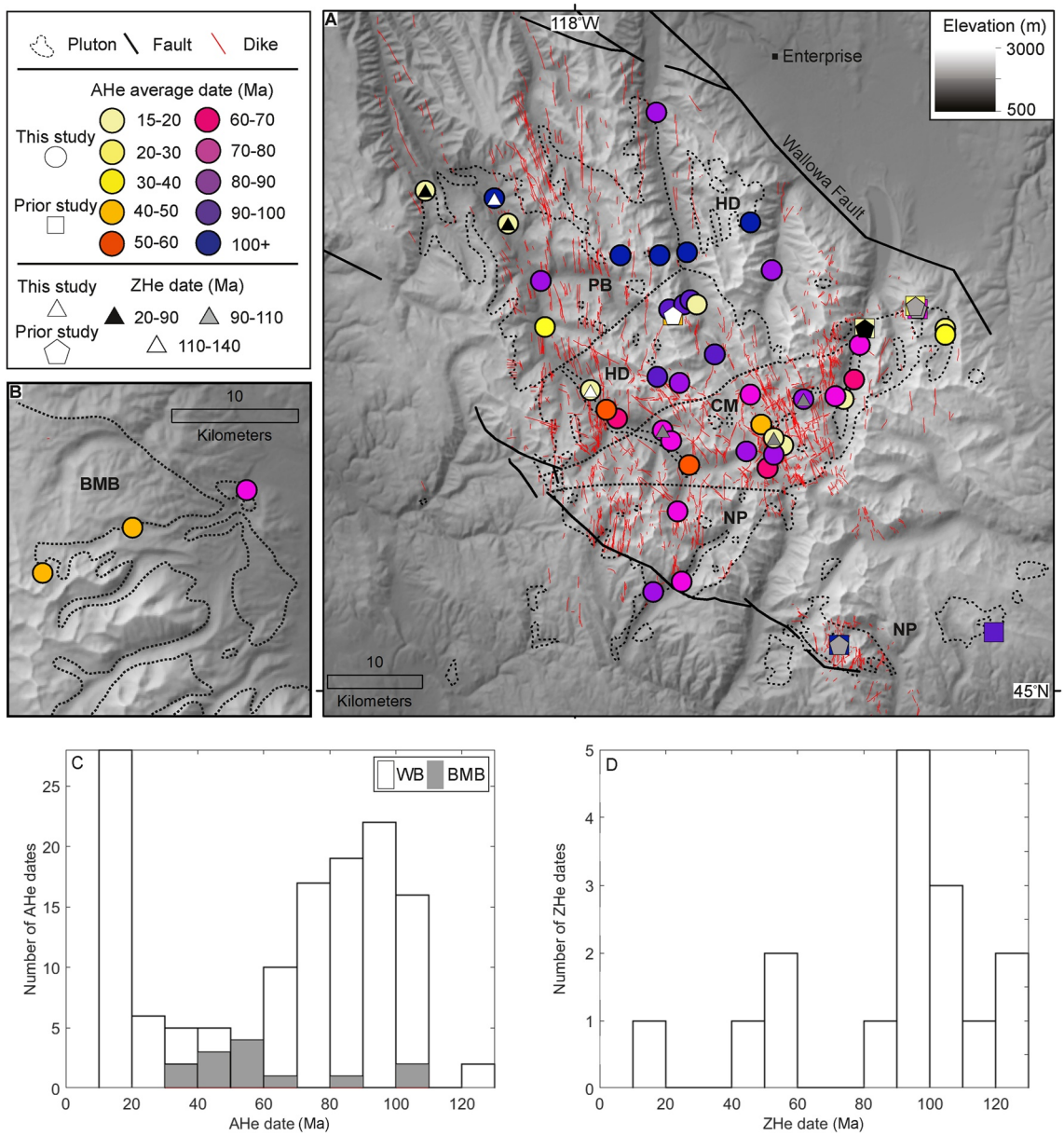

Figure 3. Low temperature thermochronometry average sample dates from (a) the Wallowa Mountains and (b) the Elkhorn Mountains. Outlines of major plutonic bodies and Chief Joseph dikes marked. Plutonic bodies from Žák et al. (2015). CM, Craig Mountain Pluton; HD, Hurricane Divide Pluton; PB, Pole Bridge Pluton; NP, Needle Point Pluton. (c) Histogram of AHe data from the Wallowa and Bald Mountain Batholiths. BMB, Bald Mountain Batholith; WB, Wallowa Batholith. (d) Histogram of ZHe data from the Wallowa Batholith.

4. Interpretation of Thermochronometry and CRB Unconformity Data

Below, we interpret the CRB unconformity and thermochronometry data for both the Elkhorn and Wallowa Mountains and their underlying batholiths. For the Wallowa batholith thermochronometry, we explore complexities introduced by thermal reheating by the Chief Joseph dikes and by differences in helium diffusivity due to sample eU. Thermal modeling of the thermochronometry data helps us to further refine our potential interpretations. We then discuss these interpretations in the context of the Cretaceous to present tectonic, topographic, and thermal histories of the Blue Mountains Province (see Section 5).

10.1029/2021TC006704

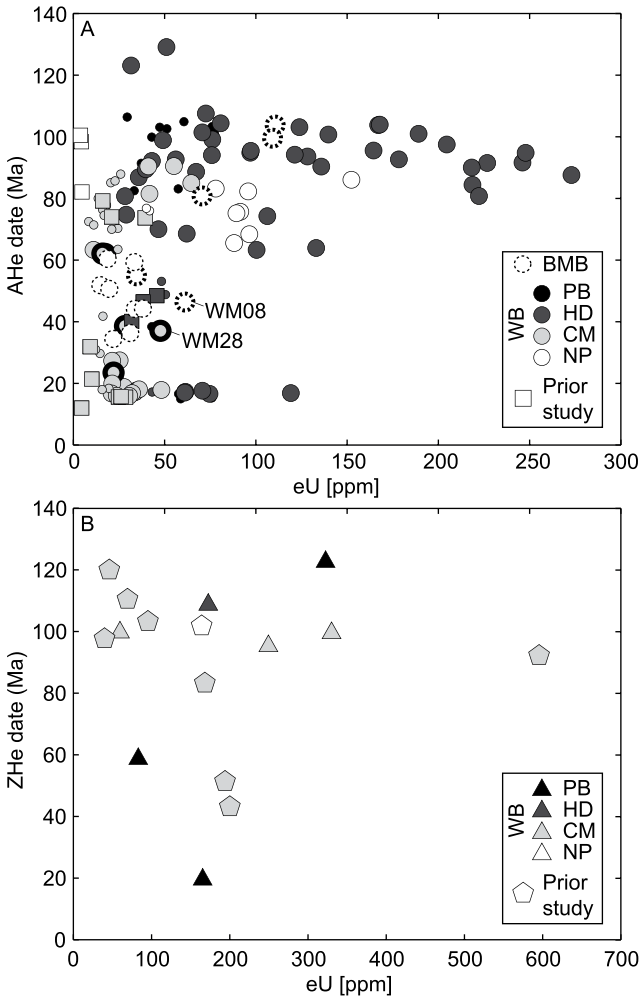

Figure 4. (a) Single grain and multigrain aliquot AHe dates from the Wallowa and Bald Mountain Batholiths plotted against eU. Multigrain aliquot dates plotted as smaller circles. (b) Single grain and multigrain aliquot ZHe dates from the Wallowa Batholith plotted against eU. All new ZHe dates presented in this study are multigrain aliquots. BMB, Bald Mountain Batholith; CM, Craig Mountain Pluton; HD, Hurricane Divide Pluton; NP, Needle Point Pluton; PB, Pole Bridge Pluton.

4.1. Elkhorn Mountains

The Elkhorn Mountains were not buried by CRB like most of the Blue Mountains Province to the east. Onlapping of younger CRB units against pre-Miocene bedrock (Figure 2a), indicates there was local topography in this region prior to the Miocene eruption of the CRB. This topography may have been significant as CRB inundated mountains with 1 km relief in the Syringa Embayment and to the southeast of the Elkhorn Mountains (Bond, 1963; Fitzgerald, 1982). Oligocene-Early Miocene andesitic-dacitic flows and pyroclastics locally fill paleo-valleys and bury 40–50 Ma fluvial units in contact with the Bald Mountain Batholith (Ferns et al., 2010; Reiners, 2005a). These deposits are boulder conglomerates distally sourced from Idaho with clasts up to 0.75 m in diameter (Allen, 1991; Dumitru et al., 2013; Reiners, 2005a), suggesting the Elkhorn Mountains did not form a barrier for east-west sediment transport in the Eocene. Therefore, it is likely the Elkhorn Mountains became a regional topographic high between the Eocene and the Miocene.

4.1.1. Bald Mountain Batholith Thermochronometry

AHe dates from the Bald Mountain Batholith are negatively correlated with elevation, with the average date of the lowest elevation sample approximately 40 Ma older than the highest elevation sample (Figure 5a). Inverted date-elevation trends like this may result from the decay of topographic relief (e.g., Braun, 2002), or the grouping of widely spaced samples across gradients in uplift rate (e.g., Reiners, 2007). The three samples from the Bald Mountain Batholith span approximately 30 km in map view (Figure 3) and extend from the western margin of the Elkhorn Mountains to the center of the range, suggesting both topographic decay and spurious correlation between samples are possible.

Because of the unusual date-elevation relationship observed in the Bald Mountain Batholith data set, we present models for each sample individually (Figure 5). Results from a model using all data can be found in Figure S9 in Supporting Information S1. Model results for samples WM06 and WM07 estimate a cooling history involving rapid cooling to near-surface temperatures after approximately 45 Ma (Figure 5b, c). The positive date-eU trend for sample WM08, however, constrains a more complicated modeled thermal history (Figure 5d). This model estimates cooling to near-surface temperatures in the Mid-Cretaceous, prior to deformation on the WISZ, followed by a period of slow reheating from approximately 40 to 80°C between 110 and 55 Ma. After 55 Ma, the model predicts steady cooling to the present.

A common feature in all thermal histories that reproduce Bald Mountain Batholith data is relatively rapid cooling in the Eocene. Regionally, the Eocene was marked by accretion of the oceanic plateau Siletzia east of the Blue Mountains Province (55–50 Ma; Wells et al., 2014), which preceded volcanism in Idaho (Challis episode 51–43 Ma; Janecke, 1994; Gaschnig et al., 2010, 2011; Chetel et al., 2011) and Oregon (Clarno volcanics 54–39 Ma; Figure 1; Retallack et al., 2000). Thermochronometry from Idaho record a phase of rapid cooling interpreted as resulting from tectonically driven unroofing during the Eocene (Fayon et al., 2017; Foster & Raza, 2002; Reiners, 2005a; Sweetkind & Blackwell, 1989). The thermal history modeled for Bald Mountain Batholith predicts a phase of post-Siletzia cooling that could reflect the onset of unroofing driven by orogeny much like in Idaho. Together with evidence for CRB onlapping, we suggest unroofing in the Eocene marks the onset of development of the modern Elkhorn Mountains.

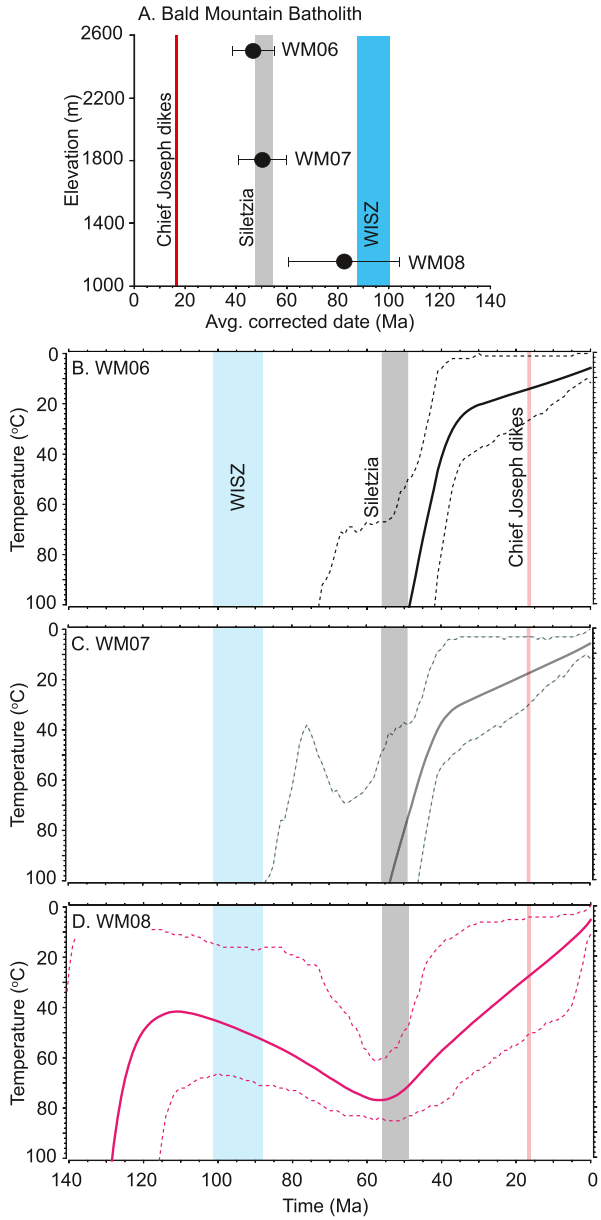

Figure 5. (a) Average corrected AHe date with 1-sigma standard deviation versus elevation plot for samples from the Bald Mountain Batholith. (b)–(d) Time-temperature inverse model results for each sample from the Bald Mountain Batholith.

4.2. Wallowa Mountains

Preserved remnants of CRB in the high peaks of the Wallowa Mountains show they were likely buried by basalt in the Miocene (Figure 2a). It is possible, however, that isolated steptoes may have remained in the central Wallowa Mountains, where fluvial deposits found beneath CRB suggest preferential preservation of Miocene valley bottoms. Generally, the limited preservation of basalt in the central Wallowa Mountains (Figures 2, S1 in Supporting Information S1) limits our ability to accurately assess local paleo-relief. On a broad scale, the structural relief on the interpolated sub-CRB unconformity across the Wallowa Mountains is similar to that of present-day topography and shows the mountains have grown in relief by approximately 2 km since 16–17 Ma (Figure 2a). Inverted CRB stratigraphy onlapping pre-Miocene bedrock to the southwest of the Wallowa Mountains and tilted flows on the flanks of the range indicate post-Miocene relief growth was localized on the Wallowa Mountains (Figure 2a). Some of this growth was aided by slip on the Wallowa Fault, with the greatest eroded depth below the sub-CRB unconformity in valleys bound by the Wallowa Fault (Figure 2b).

4.2.1. Interpreting Wallowa Batholith Thermochronometry

Interpreting thermochronometry data from the Wallowa Batholith is complicated by possible reheating during the 16–17 Ma intrusion of the Chief Joseph dike swarm (Figures 1 and 3). Both AHe and ZHe dates range from approximately 17 Ma to over 100 Ma despite being sampled in proximity (Figure 3). We can think of three possible explanations for the observed thermochronometry date spectra in the Wallowa Batholith: (a) The data could reflect the degree of helium outgassing during dike-induced reheating, with no data recording exclusively unroofing related cooling; (b) The data could exclusively reflect spatial variation in unroofing-related cooling since Cretaceous pluton emplacement; or (c) The data could reflect both the effect of unroofing-related cooling and the quantitive loss of helium following dike-induced reheating. Assuming scenario (a), thermochronometry from the Wallowa Batholith could not be analyzed for tectonic or geomorphic information. If scenario (b) is true, reheating during dike intrusion was minimal and did not result in significant helium outgassing. Scenario (c), which is our preferred interpretation, allows for data analysis both in the context of unroofing related cooling as well as dike-induced reheating.

While it is clear intrusion of the Chief Joseph dikes led to significant local thermal perturbations (Petcovic and Grunder, 2003; Reiners, 2005b; Karlstrom et al., 2019), when plotted relative to both proximity and density of mapped dikes, no clear trends in AHe and ZHe data are observed (Figure S10 in Supporting Information S1). Though we cannot parse the data set using their relationship to mapped dikes (see Text S1 in Supporting Information S1 for a more complete discussion), several observations suggest reheating during dike intrusion did not completely alter AHe and ZHe dates across the Wallowa Batholith.

Prior studies that examine the thermal effect of Chief Joseph dike intrusion on thermochronometry show that the degree of reheating is specific to the magmatic history of a dike (Karlstrom et al., 2019; Reiners, 2005b). AHe thermochronometry adjacent the Maxwell Lake dike, source of the largest single flow of CRB (Petcovic & Dufek, 2005), is reset to a distance of approximately 70 m (Karlstrom et al., 2019). The Maxwell Lake dike is anomalous among the Chief Joseph dikes because there is evidence for partial melting of the Wallowa Batholith along the dike walls (Petcovic & Grunder, 2003), suggesting reheating near this dike could represent the maximum thermal perturbation from dike intrusion. For the Lee dike, in the southern Wallowa Mountains, full helium outgassing from apatites was found to extend to a distance equivalent to two times the width of the dike

(Reiners, 2005b). Partial helium outgassing occurred over an additional distance of two dike widths. Extrapolating from this finding, partial helium outgassing from apatite would occur in samples collected within 32 m of a dike, assuming a median dike width of 8m (Morriss et al., 2020). Only five samples are this close to a mapped dike (Figure S10 in Supporting Information S1).

A small subset of samples from the Wallowa Batholith have dates between 16 and 17 Ma, which we take as evidence for complete helium outgassing at the time of Chief Joseph dike intrusion (n = 8; Figure 3c). Most samples have AHe dates between 60 and 100 Ma (n = 32), with a peak between 90 and 100 Ma (Figure 3c). ZHe dates show a similar peak between 90 and 100 Ma (Figure 3d). The overlap between AHe and ZHe date spectra is inconsistent with significant Miocene reheating because if reheating was significant, it would result in outgassing of helium from apatites before zircons and a significant difference in the relative age spectrum of the two thermchronometers. Instead, the observed date overlap is more consistent with rapid cooling between 90 and 100 Ma. Together, these observations suggest that the data set records both variation in unroofing-related cooling and Miocene dike-induced reheating.

To explore AHe and ZHe dates under the assumption that they are the product of both unroofing-related cooling and dike-induced reheating, we delineate three sample populations based on average AHe date. These populations are identified as young date (AHe date <20 Ma; n = 8), intermediate date (AHe date 20–60 Ma; n = 10), and old date (AHe date >60 Ma; n = 32) samples. From a geological perspective, we interpret these date groups as consisting of samples where helium was completely outgassed during Chief Joseph dike intrusion (young date samples), samples that experienced partial helium outgassing during dike intrusion (intermediate date samples), and samples that experienced little to no helium outgassing during dike intrusion (old date samples). Interpreting young date samples as having experienced complete helium outgassing during dike intrusion is well supported by their relatively uniform date spectrum. The boundary we choose between the intermediate date and old date samples is more arbitrary, but is placed near the minimum in the date-frequency distribution (Figure 3a). In our exploration of the data we find the distinction between intermediate and old date samples is a functional approximation for the impact of dike-induced reheating and that old date samples have a date spectrum consistent with unroofing-related cooling.

4.2.2. Spatial Trends in AHe and ZHe Dates

Plotting AHe and ZHe data relative the sub-CRB unconformity as well as present-day elevation supports the interpretation that the data set contains both Miocene reheating and unroofing-related cooling signals (Figure 6). While it is likely that estimated depths relative to the sub-CRB unconformity are underestimated for samples far from CRB outcrops (Figure S1 in Supporting Information S1), we regard distance from the sub-CRB unconformity as a more consent metric for vertical distance between samples than present-day elevation. This is because depth below the sub-CRB unconformity accounts for surface warping evidenced by cross-sections of topography and CRB (Figure 2).

When plotted relative to depth as well as present-day elevation we observe a consistent positive slope across all four plutons in old AHe date samples, suggesting they record a unroofing-related cooling signal. For intermediate and young AHe date samples there are no clear trends. The subtle difference between plots of date versus elevation or depth below CRB reflect the similarity in present-day topographic trends with the sub-CRB unconformity across the central and south-eastern Wallowa Mountains (Figure 2).

4.2.2.1. Young Date Samples

Young AHe and ZHe date samples have a relatively consistent AHe date spectrum between 15 and 20 Ma across their range of depths and elevations (Figure 6). ZHe dates for these samples vary from approximately 20 to 100 Ma, reflecting different degrees of helium outgassing due to heterogeneous Miocene reheating. The lack of AHe dates <15 Ma shows that all young date samples rapidly cooled below the apatite closure temperature following dike-induced reheating. This limits the potential for prolonged reheating by CRB burial, which has been found to produce younger AHe dates in samples collected elsewhere in the Blue Mountains (e.g., Kahn et al., 2020). From this we infer that either the Wallowa Batholith was not buried by the entire 1 km stratigraphic thickness of CRB, as this would result in sample depths of approximately 2 km and ambient temperatures great enough to allow continued helium diffusion, or unroofing (and cooling) commenced immediately following CRB burial.

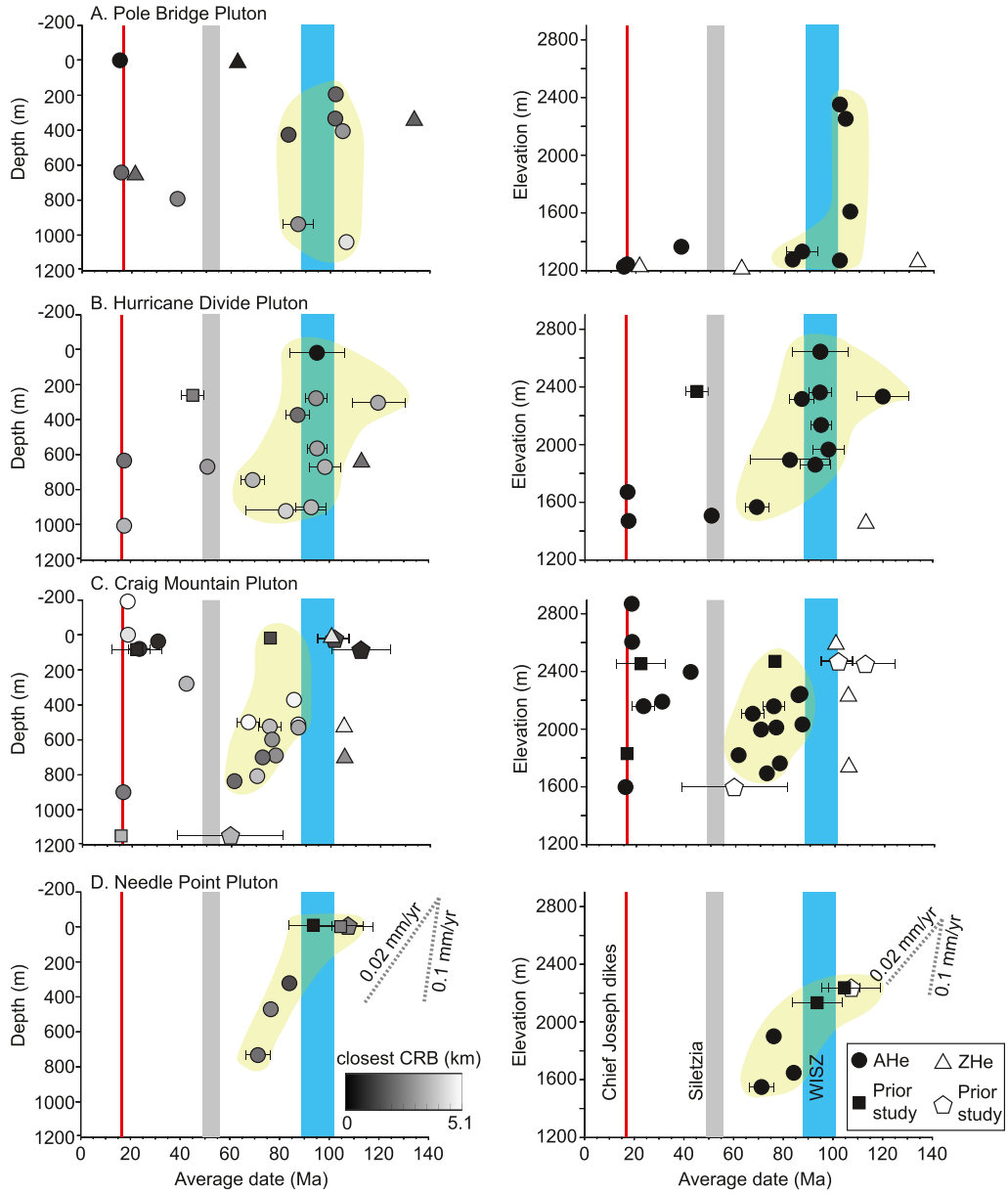

Figure 6. Average corrected AHe dates with 1-sigma standard deviation plotted relative to the sub-CRB unconformity and present-day elevation for Wallowa Batholith plutons. Dates colored by distance from nearest preserved CRB when plotted relative to depth below the sub-CRB unconformity. Timing of Chief Joseph dike intrusion, Siletzia accretion, and peak WISZ activity marked by red, gray, and blue bars, respectively. Old date samples outlined in yellow.

4.2.2.2. Old Date Samples

AHe dates in the old date sample population are generally correlated with the time of activity in the WISZ while ZHe dates mostly predate or coincide with the onset of the WISZ. Approximate AHe date-depth/elevation trends vary from 0.1 mm/yr from the Pole Bridge to 0.02 mm/yr for the Needle Point Pluton (Figure 6). Steeper date-depth/elevation trends are observed in AHe dates coincident with WISZ activity, while those that postdate WISZ activity have shallower date-depth/elevation trends. If these date-depth/elevation trends are a record of unroofing-related cooling, then we interpret them as showing high cooling rates during deformation in the WISZ, which decrease after cessation of WISZ activity approximately 88 Ma. Although the most significant unroofing associated with the WISZ occurred in the Salmon River Suture Zone and east of the WISZ (Giorgis et al., 2005;

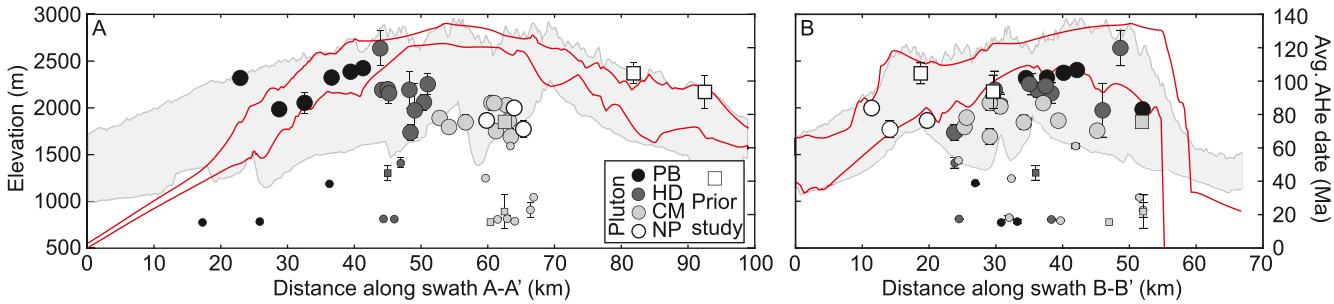

Figure 7. Average corrected AHe dates with 1-sigma standard deviation plotted along the swaths A–A′ and B–B′ (Figure 2). Symbols are smaller for samples with likely He loss due to dike reheating. In panels A and B, samples are colored by pluton where, PB, Pole Bridge Pluton; HD, Hurricane Divide Pluton; CM, Craig Mountain Pluton; NP, Needle Point Pluton and plotted against topography (gray) and CRB basal unconformity (red). Samples outside the width of measured swaths were projected onto the swath.

Kahn et al., 2020; Lund & Snee, 1988), these observations indicate unroofing rates also remained elevated in the Wallowa Batholith.

Differences in the AHe date spectrum across the Wallowa Batholith suggest differences in cooling since the Late-Cretaceous. Younger AHe dates are recorded in the Craig Mountain and Needle Point plutons than in the Hurricane Divide and Pole Bridge plutons (Figure 6). These date trends may be due to differences in the magnitude of Late-Cretaceous to present unroofing. This could reflect the transition from a tectonically driven cooling signal, preserved in AHe data from the Pole Bridge pluton, to an unroofed late-Cretaceous and Cenozoic AHe partial retention zone in the Craig Mountain and Needle Point plutons (e.g., Crowley et al., 2002; Wolf et al., 1998). A correlation between AHe dates in the Wallowa Batholith and the gross topography of the Wallowa Mountains suggests present-day topography reflects long-term trends in cooling (Figure 7). If older AHe dates reflect cooling from unroofing, this indicates the areas with highest topography today and greatest upwarping of the sub-CRB unconformity also experienced the greatest unroofing since the Late-Cretaceous. However, variation in sample eU, with lowest eU values consistently found in the central Wallowa Mountains (Figure S11 in Supporting Information S1), make the comparison of AHe dates suspect.

AHe dates tend to be relatively uniform for each pluton when plotted relative to distance from the Wallowa Fault (Swath B-B′, Figure 7b). The lack of discernible trends suggest the Wallowa Fault was not instrumental in driving the cooling recorded by samples. If the fault did aid in cooling of the batholith to near-surface temperatures, AHe dates would be younger near the fault. This is not observed, indicating the batholith was already near the surface when the fault initiated.

4.2.3. Wallowa Batholith Thermal History Models

Spatial trends in AHe dates from old date samples (Figures 6 and 7), allude to pre-Miocene topographic development of the Wallowa Mountains region. However, sample-specific helium diffusivity driven by differences in sample eU (Figure 4) complicates interpretation of these data. To resolve this issue, we used the software QTQt to estimate viable time-temperature histories for each pluton in the Wallowa Batholith. Four suites of inverse models were run for each pluton in the Wallowa Batholith, a model suite including only old date samples modeled relative to present-day elevation, one with only old date samples modeled relative to depth below the sub-CRB unconformity (Figure 8), a suite with both old and intermediate date samples (Figure S12 in Supporting Information S1), and a suite with all samples (Figure S13 in Supporting Information S1). An underlying assumption in all models is that input samples share a common cooling history. While this assumption may prove problematic (e.g., Schildgen et al., 2018), it has proven effective if applied locally (e.g., Collett et al., 2019; Zapata et al., 2019). We gauge the validity of estimated time-temperature histories by their ability to reproduce the observed data.

Our preferred model suite including only old date samples modeled relative to depth below the sub-CRB unconformity (Figure 8). These models successfully reproduce the input data with similar time-temperature histories across all plutons and also incorporate paleo-topographic constraint provided by the sub-CRB unconformity. Models using present-day elevations and only old-age samples are comparable to our preferred models both in terms of estimated time-temperature histories and accuracy of helium date observations (Figure S13 in Supporting Information S1). Models using intermediate and young dates, however, cannot successfully predict observed

10.1029/2021TC006704

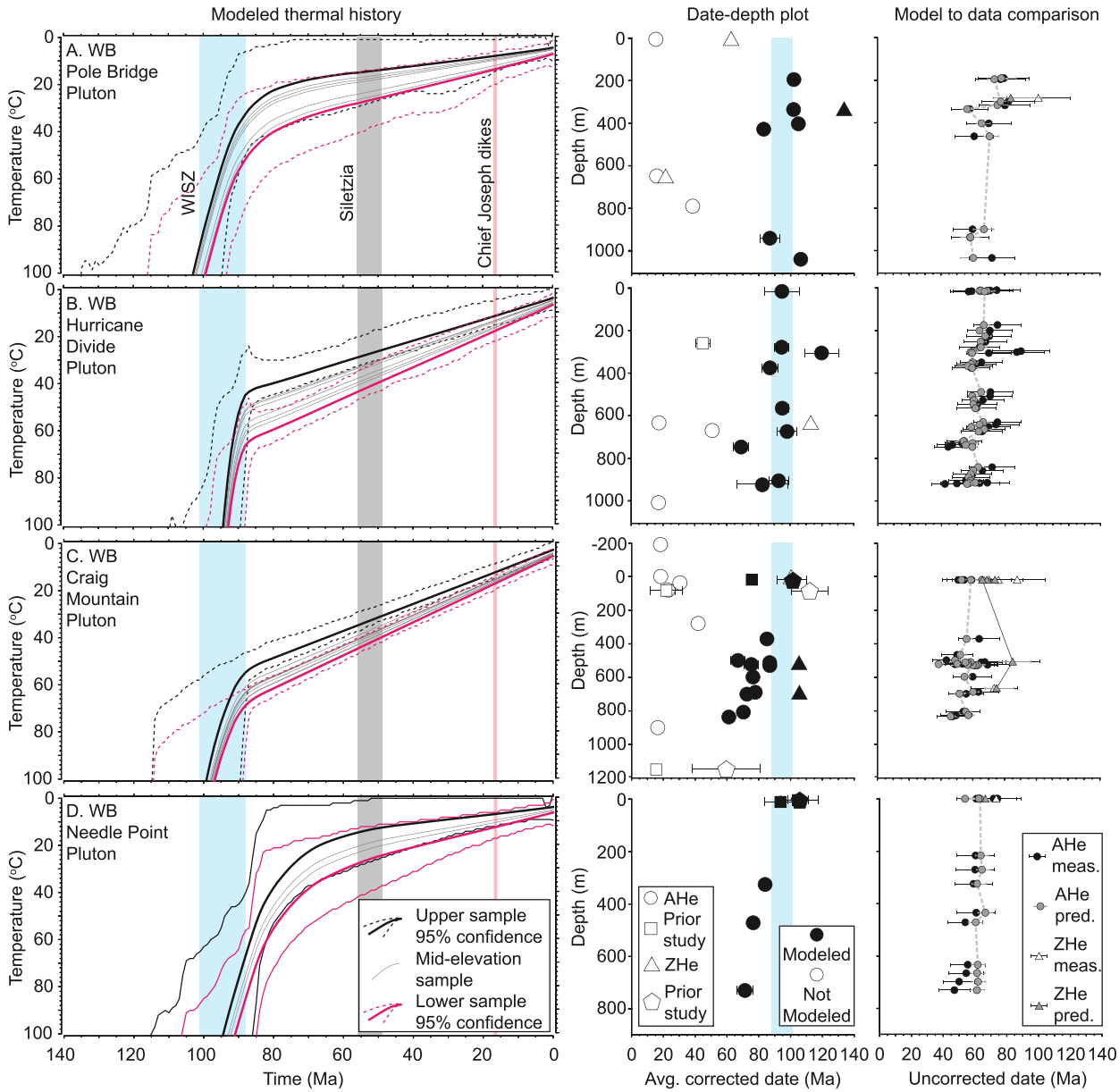

Figure 8. Time-temperature inverse model results for sampled plutons from the Wallowa Batholith. Left: Time-temperature inverse model results for sampled plutons from the Wallowa Batholith. Weighted mean modeled time-temperature history for each pluton is shown as is an average sample date with 1-sigma standard deviation. Middle: Age versus depth plot. Right: Comparison between the modeled AHe and ZHe dates and error and the measured dates with an applied 10% error. Dates are modeled relative to the sub-CRB unconformity.

data (Figures S14 and S15 in Supporting Information S1). The preferred models estimate rapid cooling to the end of activity on the WISZ in the Mid- to Late-Cretaceous, followed by slow, steady, cooling to the present (Figures 8a–8d). A similar thermal history is also estimated by the Hurricade Divide and Craig Mountain Pluton models when present-day elevation is used in place of depth below the sub-CRB unconformity (Figure S13b, c in Supporting Information S1). That a Cretaceous inflection in cooling rate is observed across models using depth below the sub-CRB unconformity and in half of the models using present-day elevation gives us confidence that the old date samples retain a cooling signal driven by unroofing. Furthermore, the correlation between this timing and the end of activity on the WISZ provides an explanation for the estimated thermal histories.

In our preferred models, modeled cooling rates are 4–6°C/Myr during peak WISZ activity for the Pole Bridge, Craig Mountain and Needle Point plutons which have ZHe data that constrain higher temperatures and 15°C/Myr

for the Hurricane Divide Pluton which does not include higher-temperature constraint from ZHe data. Models for the Pole Bridge, Hurricane Divide, and Craig Mountain plutons all estimate a sudden decrease in cooling rate between 90 and 80 Ma, immediately following activity in the WISZ (Figures 8a–8c), whereas modeled cooling rates for the Needle Point Pluton are less well constrained and allow for slow cooling through the Late Cretaceous (Figure 8d).

By 80 Ma, the uppermost sample from the Pole Bridge Pluton is modeled to have cooled to approximately 20°C, while the uppermost sample in the Hurricane Divide Pluton cooled to approximately 40°C, the Craig Mountain Pluton cooled to approximately 50°C, and the Needle Point Pluton cooled to approximately 40°C. Cooling rates from the Mesozoic to present are predicted to have been highest in the Craig Mountain Pluton (0.5–0.7°C/Ma) and lowest in the Pole Bridge Pluton (0.2–0.4°C/Ma). These rates are an order of magnitude slower than those predicted during WISZ activity. They also suggest different scales of Mesozoic to present unroofing across the Wallowa Batholith. Assuming a 20–30°C/km geothermal gradient, model results show 1–1.5 km more unroofing of the Craig Mountain Pluton than the Pole Bridge Pluton from 80 Ma to the present.

The modeled Cenozoic thermal history for all plutons involves monotonic cooling to the present (Figure 8). While this estimate is probably too simplistic, it does show that, within the resolution of the AHe and ZHe thermochronometers, there were no major reheating or cooling episodes during this time. Using present-day elevation instead of depth below the sub-CRB unconformity results in an estimated increase in cooling rate at approximately 50 Ma for the Pole Bridge Pluton (Figure S13a in Supporting Information S1), however, this model does not successfully reproduce input data. Montonic cooling during the Cenozoic could be due to low model resolution in the Cenozoic because of only using samples with AHe dates >60 Ma in our preferred models but models including intermediate date or all samples poorly reproduce observed AHe and ZHe dates and estimate multiple, geologically unreasonable, Cenozoic reheating episodes (Figures S14, S15 in Supporting Information S1).

Taken together, modeling results corroborate our interpretation of trends in old AHe dates across the batholith as reflecting differences in net unroofing since the Cretaceous rather than variations in dike-related heating. They indicate that the Craig Mountain Pluton, exposed in the center of the Wallowa Mountains (Figure 3), has experienced the greatest amount of Cretaceous to present cooling among all the sampled plutons. While forward modeling shows it is possible the low eU values for AHe samples from the Craig Mountain Pluton increase their sensitivity to Miocene reheating (Figure S11 in Supporting Information S1), we consider the greater estimated post-Cretaceous cooling in the Craig Mountain Pluton relative to the rest of the Wallowa Batholith a robust result.

5. Discussion

AHe and ZHe thermochronometry from the Wallowa and Bald Mountain Batholiths combined with thermal modeling and map interpretation of the CRB basal unconformity provides insight into the tectonic, topographic, and thermal history of the Blue Mountains Province. The results from this study suggest that the Bald Mountain and Wallowa Batholiths have distinct thermal and topographic histories resulting from the varying influence of three significant periods of tectonic and volcanic activity: (a) Cretaceous terrane accretion followed by transpression along the WISZ, (b) Eocene unroofing in the Elkhorn Mountains following the accretion of Siletzia, and (c) Miocene dike intrusion and subsequent relief generation in the Wallowa Mountains. Below, we review each of these time periods.

5.1. Rapid Mesozoic Cooling of the Wallowa and Bald Mountain Batholiths

Thermal models predict cooling of the Wallowa and Bald Mountain Batholiths began immediately following emplacement (Figures 5 and 8). Cooling was likely driven by unroofing resulting from crustal thickening during plutonism in the latter stages of terrane amalgamation and accretion to North America (Schwartz et al., 2011, 2014; Žák et al., 2015), and by shortening during transpression along the WISZ (Figure 9; A. Giorgis et al., 2005, 2008). Thermal models for the Bald Mountain Batholith suggest cooling to the near surface predates transpression on the WISZ (Figure 5d), whereas models from the Wallowa Batholith show a decrease in cooling rate shortly after the end of WISZ activity (Figures 8a–8d). A similar increase in the influence of the WISZ from west to east across the Blue Mountains Province is observed by Kahn et al. (2020).

10.1029/2021TC006704

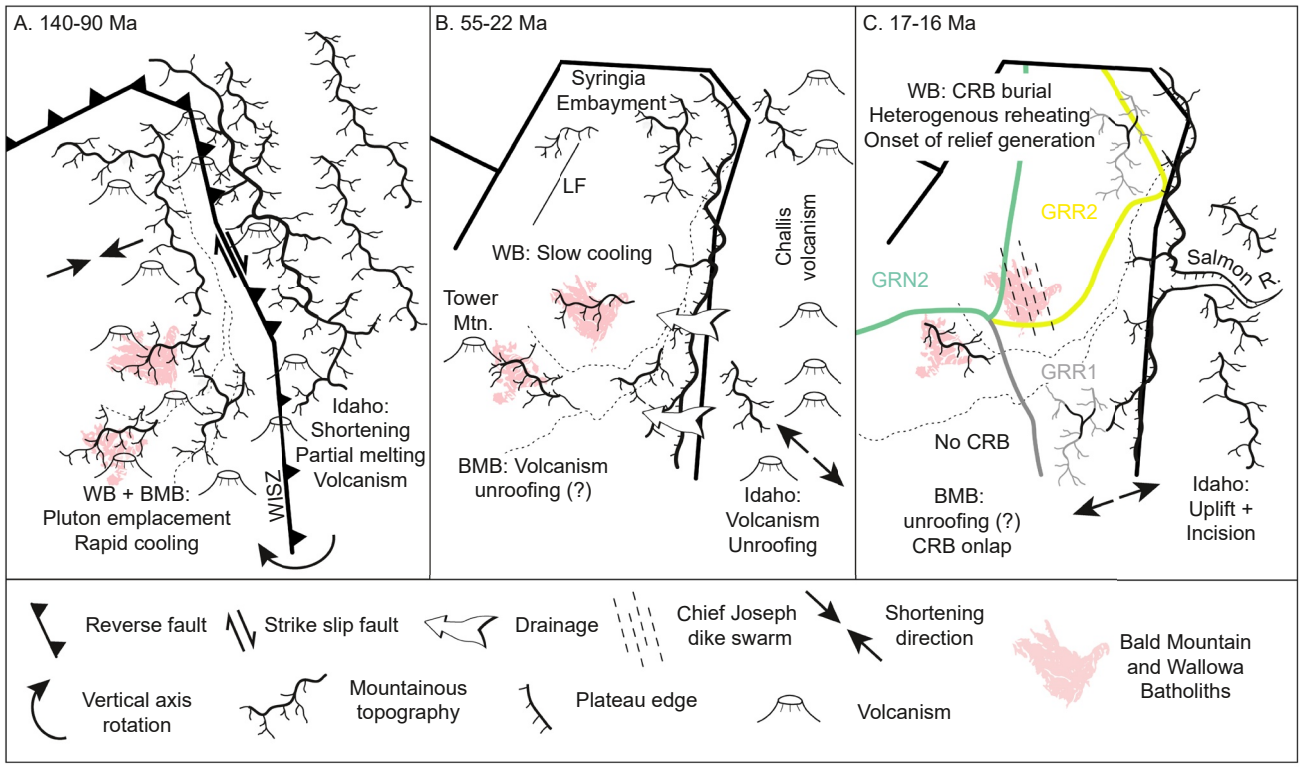

Figure 9. Summary cartoon showing proposed tectonic, volcanic, and geomorphic history for the study area and surroundings. Panels focus on time periods important in the thermal histories predicted by thermochronometry. BMB, Bald Mountain Batholith; IB, Idaho Batholith; WB, Wallowa Batholith.

By the end of transpression on the WISZ around 88 Ma, both the Wallowa and Bald Mountain Batholiths had cooled to near surface temperatures (Figure 5d). The abrupt inflection in cooling rate observed across many modeled time-temperature histories likely reflects the cessation of a tectonic driver for unroofing. Alternatively, exposure at the surface of the less erodible batholiths may have resulted in a decreased unroofing rate (Flowers & Ehlers, 2018). However, landscapes have a propensity to adjust toward a steady state between uplift and erosion (e.g., Willett & Brandon, 2002), and reduced cooling rates resulting from decreased bedrock erodibility would only persist over the time of landscape adjustment. A lack of increase in cooling rate after 90 Ma in the absence of reheating is inconsistent with a transient reduction in cooling rate following surface exposure of the batholiths. Therefore, it is more likely that the Mid-Cretaceous decrease in cooling rate modeled for the Wallowa and Bald Mountain Batholiths resulted from the cessation of tectonically driven uplift following terrane accretion and WISZ activity.

Cooling rates remained slow from the Mid-Late Cretaceous to the Eocene for the Bald Mountain Batholith and until at least the Miocene for the Wallowa Batholith (Figure 7). Subtle differences in modeled cooling rate between plutons in the Wallowa Batholith suggest differential post-Cretaceous net-unroofing across the batholith. The cooling trends we observe in the Wallowa Batholith could be due to the decay of orogenic topography since the Crecateous. Similar trends in thermochronometry have been observed where relief established during uplift results in greater postorogenic unroofing in the center of mountain ranges (Reiners, 2003), and postorogenic relief decay (Braun, 2002). Alternatively, trends in AHe date across the Wallowa Batholith could be due to isostatically derived upwarping. Such a scenario is theoretically possible if there is a significant difference in bedrock density between the batholith and surrounding rocks (e.g., Braun et al., 2014). However, the metavolcanic and metasedimentary bedrock of the Wallowa Terrane is likely to have a similar density to the granodiorite of the Wallowa Batholith. Furthermore, AHe date trends would be expected to be radially distributed around the center of the Wallowa Batholith, with the youngest in the center of the exposed batholith (e.g., Braun et al., 2014). This is not observed, instead the youngest AHe dates are found near the eastern margin of the exposed batholith.

Regionally, unroofing and deformation continued through the Mesozoic into the Cenozoic. North of the Wallowa Batholith, the dextral-oblique Mt Idaho and Limekiln structural zones in the Syringa Embayment may have remained active until approximately 70 Ma (Figure 1; Schmidt et al., 2017). In the WISZ and to the east, unroofing rates remained elevated through the early Cenozoic, with up to 5 km of unroofing between the late Cretaceous and the Eocene in central Idaho (Fayon et al., 2017; Giorgis et al., 2005), driven by ongoing tectonic deformation, volcanism, and the growth of an orogenic plateau. Evidence for an orogenic plateau is specifically linked with the emplacement and unroofing history of the Idaho Batholith (Fayon et al., 2017). Neither the Wallowa and Bald Mountain Batholiths record cooling associated with this period of unroofing in Idaho, supporting prior conclusions that the topographic growth and plutonism associated with the emplacement of the Idaho Batholith in interior Idaho did not extend west of the WISZ into the Blue Mountains Province (Fayon et al., 2017; Gaschnig et al., 2017). This distinct thermal history between the regions west and east of the WISZ, while partly associated with regional trends in volcanism, also indicates orogenic plateau growth may have been relegated to points east of the WISZ (Fayon et al., 2017).

5.2. Renewed Eocene Cooling of the Bald Mountain Batholith

Inverse models of thermochronometry from the Bald Mountain Batholith estimate cooling following the Eocene accretion of the oceanic plateau Siletzia (Figures 5b–5d). Cooling may have been associated with a period of unroofing driven by regional tectonics and volcanism. In Idaho, the Eocene is marked by a phase of rapid unroofing and volcanism and the persistence of an orogenic plateau (Fayon et al., 2017). Sediments derived from Eocene unroofing in Idaho are preserved beneath volcanic units associated with the 32-22 Ma Tower Mountain Caldera over the Bald Mountain Batholith (Ferns et al., 2010; Reiners, 2005a; Seligman et al., 2014). The age of these units attests to surface exposure of the batholith between 40 and 32 Ma. Furthermore, the Idaho source of the fluvial deposits suggests that topographic growth in the Elkhorn Mountains was not initially substantial enough to disrupt Eocene drainage patterns. Later volcanic units associated with the Tower Mountain Caldera (Figures 1 and 9b), are andesitic-dacitic flows and pyroclastics which locally fill paleo-valleys along the northern margins of the Elkhorn Mountains (Ferns et al., 2010), suggesting that by this time, there was substantial local relief. These observations, together with the lack of CRB preserved across much of the Elkhorn Mountains and thermal model results, suggest that the modern Elkhorn Mountains likely formed shortly after the accretion of Siletzia (Figure 9b).

5.3. Miocene to Present Evolution of the Wallowa and Elkhorn Mountains

The topographic development of the Wallowa and Elkhorn Mountains from the Miocene to present is the product of regional deformation and the onset of alpine glaciation. Post-Miocene deformation is most clearly recognizable in the distribution of CRB (Figures 2 and 9; Hales et al., 2005). Regional deformation of the southern part of the study area likely began during the earliest phases of CRB eruption, with uplift leading to northwestward offlap of the younger Grande Ronde R2 and N2 members (Figure 9c; Camp, 1995). This uplift may have been aided by deformation on discreet faults including the Wallowa and Limekiln Faults (Camp & Hooper, 1981; Reidel et al., 2013), as well as long wavelength uplift due to delamination of underlying mantle lithosphere or lower crust (Camp & Hanan, 2008; Hales et al., 2005). While relief across the Elkhorn Mountains was most likely already substantial by the Miocene, almost 2.5 km of relief on the sub-CRB unconformity across the Wallowa Mountains attests to significant relief growth since the Miocene (Figure 2a). This relief developed in part by motion on the Wallowa Fault and resulted in the incision of deep valleys into the Wallowa Batholith (Figure 2b). The Miocene to present increase in relief in the Wallowa Mountains independent of the Elkhorn Mountains, is consistent with the hypothesis derived from upper-mantle seismic tomography, that the Wallowas were isostatically uplifted due to the development of a lithospheric instability or delamination event in the Miocene (Darold & Humphreys, 2013; Hales et al., 2005). Regional crustal anisotropy further suggests crustal deformation in Northeastern Oregon is linked to upper mantle density variation (Castellanos et al., 2020), consistent with recent lithosphere-scale deformation. Nonetheless, our data set cannot validate whether the Wallowa Mountains were uplifted due to these processes, with any mechanism resulting in local post-Miocene uplift being acceptable.

The scale of post-Miocene unroofing in the Wallowa Mountains can be roughly estimated as not exceeding approximately 1.25 km depth below the sub-CRB unconformity (Figure 2b). However, given the lower certainty of the elevation of the sub-CRB unconformity in the central Wallowa Mountains, it is possible the contact interpolation represents a minimum elevation in this area. If this is the case, then the central Wallowa Mountains may have experienced greater post-Miocene unroofing than the sub-CRB unconformity would suggest. Such a scenario is consistent with spatial trends in AHe date across the Wallowa Mountains (Figure 7a) as well as differences in estimated net-cooling since the Cretaceous for plutons in the Wallowa Batholith (Figure 8). These data indicate the central Wallowa Mountains have experienced greater unroofing than the flanks of the range since the Cretaceous. While we cannot parse whether this is the product of long term differences in unroofing rate since the Cretaceous or a more recent development, our data invite the possibility that post-Miocene unroofing of the Wallowa Batholith is greater than 1.25 km.

Further isostatic uplift and valley deepening and widening during alpine glaciation contributed to the present-day topography of both the Wallowa and Elkhorn Mountains. In the Wallowa Mountains, valleys that cross the Wallowa Fault show significant evidence for deepening and widening due to glaciation (Figure 2b). The effect of glaciation on the geomorphology of both ranges has resulted in topographic similarity between each mountain range despite their differing unroofing histories.

6. Conclusions

New geologic map interpretations and low temperature thermochronometry data from the Blue Mountains Province reveal multipart thermal and unroofing histories for the Wallowa and Bald Mountain Batholiths and shed light on the topographic development of the Wallowa and Elkhorn Mountains. Despite the potential for helium outgassing following dike-induced reheating in the Wallowa Batholith, many samples still record a cooling signal associated with unroofing. By limiting interpretation to samples that are more likely to record this cooling signal, we evaluated the thermochronometry in the context of landscape development. Cooling of the Wallowa and Bald Mountain Batholiths began immediately following emplacement. Rapid cooling of the Bald Mountain Batholith predated peak activity on the WISZ and was likely related to erosional unroofing following crustal thickening during the late stages of terrane amalgamation and accretion to North America. Rapid cooling of the Wallowa Batholith ceased immediately following activity on the WISZ, indicating that transpression led to crustal shortening and erosional unroofing within the eastern Blue Mountains Province as well as east of the terrane-continent suture. We suggest that by the Late-Cretaceous both the Wallowa and Elkhorn Batholiths had cooled to near-surface temperatures.

The Bald Mountain Batholith may have experienced a period of slow reheating in the Late-Cretaceous and early Cenozoic followed by cooling in the Eocene that we propose is linked to the development of the modern Elkhorn Mountains. The Wallowa Batholith cooled slowly through much of the Cenozoic with subtle evidence for a proto-Wallowa Mountains or differential post-Miocene unroofing revealed in cooling trends across the batholith. During Miocene CRB eruption, Eocene-age topography in the Elkhorn Mountains prevented their burial. However, CRB did inundate the exhumed Wallowa Batholith. Moreover, Miocene to present deformation, evidenced by warping and faulting of CRB, attests to approximately 2 km of relief generation in the Wallowa Mountains and an indeterminant amount in the Elkhorn Mountains. The relief on the sub-CRB unconformity across the Wallowa Mountains is only slightly greater than present topography, indicating the modern Wallowa Mountains formed from the Miocene to the present.

Our results show that the Wallowa and Elkhorn Mountains have distinct topographic and thermal histories consistent with models for localized Miocene uplift of the Wallowa Mountains. The distinctions in topographic and thermal histories stem from the waning westward influence of WISZ deformation in the Blue Mountains Province, localized volcanism and deformation following the Eocene accretion of Siletzia, the Miocene eruption of CRB via the Chief Joseph dikes, and Miocene to present relief generation.

Data Availability Statement

Data associated with this paper can be found at https://doi.org/10.5281/zenodo.5839115.

Acknowledgments
The authors thank Cody Mack, Kristin Beck, Camille Colette, Bradly Markle, Nathaniel Schoettle-Greene, Sean Lahusen, Laeben Lester, Brad Wakoff, and Greg Gerbi for field work assistance. The authors thank the United States Forest Service for granting permission to sample rocks in the Eagle Cap Wilderness. The authors thank Gene Humphreys, Jonathan Perry-Houts, Matthew Morris, Brian Yanites, Nate Mitchell, Leif Karlstrom, Kendra Murray, and Basil Tikoff for valuable discussions regarding the study area. This paper was greatly improved by comments and recommendations by Joshua Schwartz, William Guenthner, Jessica Stanley and associate editor Robinson Cecil. Grik Dubin provided invaluable assistance with numerical modeling. The authors thank Ken Farley and Peter Reiners for assistance with He thermochronology analysis. The authors appreciate funding support from the University of Washington Royalty Research Fund and NSF EAR-1727046 to Duvall. Mineral separation was conducted at GeoSep Services with help from Jim, Charlie, Victoria, and Paul O'Sullivan.

References

Allen, J. (1991). The case of the inverted auriferous paleotorrent—Exotic quartzite gravels on Wallowa Mountain peaks. *Oregon Geology*, *53*(5), 104–107.

Ault, A. K., Flowers, R. M., & Bowring, S. A. (2013). Phanerozoic surface history of the Slave craton. *Tectonics*, *32*(5), 1066–1083. https://doi.org/10.1002/tect.20069

Ault, A. K., Gautheron, C., & King, G. E. (2019). Innovations in (U–Th)/He, fission track, and trapped charge thermochronometry with applications to earthquakes, weathering, surface-mantle connections, and the growth and decay of mountains. *Tectonics*, *38*(11), 3705–3739. https://doi.org/10.1029/2018TC005312

Bond, J. (1963). *Geology of the clearwater embayment (Pamphlet No. 128)*. Idaho Bureau of Mines.

Braudy, N., Gaschnig, R. M., Wilford, D., Vervoort, J. D., Nelson, C. L., Davidson, C., et al. (2017). Timing and deformation conditions of the western Idaho shear zone, West Mountain, west-central Idaho. *Lithosphere*, *9*(2), 157–183. https://doi.org/10.1130/L519.1

Braun, J. (2002). Quantifying the effect of recent relief changes on age–elevation relationships. *Earth and Planetary Science Letters*, *200*(3), 331–343. https://doi.org/10.1016/S0012-821X(02)00638-6

Braun, J., Simon-Labric, T., Murray, K. E., & Reiners, P. W. (2014). Topographic relief driven by variations in surface rock density. *Nature Geoscience*, *7*(7), 534–540. https://doi.org/10.1038/ngeo2171

Brown, S. J., Thigpen, J. R., Spotila, J. A., Krugh, W. C., Tranel, L. M., & Orme, D. A. (2017). Onset timing and slip history of the Teton fault, Wyoming: A multidisciplinary reevaluation: Timing of onset of the Teton fault. *Tectonics*, *36*(11), 2669–2692. https://doi.org/10.1002/2016TC004462

Burns, E. S., Morgan, D. S., Peavler, R. S., & Kahle, S. C. (2011). Three-dimensional model of the geologic framework for the Columbia Plateau regional aquifer system, Idaho, Oregon, and Washington. USGS Scientific Investigations Report No. 2010–5246.

Camp, V. E. (1995). Mid-Miocene propagation of the Yellowstone mantle plume head beneath the Columbia River basalt source region. *Geology*, *23*(5), 4. https://doi.org/10.1130/0091-7613(1995)023<0435:mmpoty>2.3.co;2

Camp, V. E., & Hanan, B. B. (2008). A plume-triggered delamination origin for the Columbia River basalt group. *Geosphere*, *4*(3), 480. https://doi.org/10.1130/GES00175.1

Camp, V. E., & Hooper, P. R. (1981). Geologic studies of the Columbia plateau: Part I. Late Cenozoic evolution of the southeast part of the Columbia River basalt province. *GSA Bulletin*, *92*(9), 659–668. https://doi.org/10.1130/0016-7606(1981)92<659:gsotcp>2.0.co;2

Castellanos, J. C., Perry-Houts, J., Clayton, R. W., Kim, Y., Stanciu, A. C., Niday, B., & Humphreys, E. (2020). Seismic anisotropy reveals crustal flow driven by mantle vertical loading in the Pacific NW. *Science Advances*, *6*(28). eabb0476. https://doi.org/10.1126/sciadv.abb0476

Chetel, L. M., Janecke, S. U., Carroll, A. R., Beard, B. L., Johnson, C. M., & Singer, B. S. (2011). Paleogeographic reconstruction of the Eocene Idaho river, north American Cordillera. The *Geological Society of America Bulletin*, *123*(1–2), 71–88. https://doi.org/10.1130/B30213.1

Clark, M. K., Royden, L. H., Whipple, K. X., Burchfiel, B. C., Zhang, X., & Tang, W. (2005). Late Cenozoic uplift of southeastern Tibet. *Geology*, *33*(6), 4. https://doi.org/10.1130/g21265.1

Collett, C. M., Duvall, A. R., Flowers, R. M., Tucker, G. E., & Upton, P. (2019). The timing and style of oblique deformation within New Zealand's Kaikōura ranges and Marlborough fault system based on low-temperature thermochronology. *Tectonics*, *38*(4), 1250–1272. https://doi.org/10.1029/2018TC005268

Crowley, P. D., Reiners, P. W., Reuter, J. M., & Kaye, G. D. (2002). Laramide exhumation of the Bighorn Mountains, Wyoming: An apatite (U-Th)/He thermochronology study. *Geology*, *30*(1), 4. https://doi.org/10.1130/0091-7613(2002)030<0027:leotbm>2.0.co;2

Darold, A., & Humphreys, E. (2013). Upper mantle seismic structure beneath the Pacific northwest: A plume-triggered delamination origin for the Columbia River flood basalt eruptions. *Earth and Planetary Science Letters*, *365*, 232–242. https://doi.org/10.1016/j.epsl.2013.01.024

Dumitru, T. A., Ernst, W. G., Wright, J. E., Wooden, J. L., Wells, R. E., Farmer, L. P., et al. (2013). Eocene extension in Idaho generated massive sediment floods into the Franciscan trench and into the Tyee, Great Valley, and Green River basins. *Geology*, *41*(2), 187–190. https://doi.org/10.1130/G33746.1

Ehlers, T. A., & Farley, K. A. (2003). Apatite (U–Th)/He thermochronometry: Methods and applications to problems in tectonic and surface processes. *Earth and Planetary Science Letters*, *206*(1–2), 1–14. https://doi.org/10.1016/S0012-821X(02)01069-5

Fayon, A. K., Tikoff, B., Kahn, M., & Gaschnig, R. M. (2017). Cooling and exhumation of the southern Idaho batholith. *Lithosphere*, *9*(2), 299–314. https://doi.org/10.1130/L565.1

Ferns, M. L., & McClaughry, J. D. (2013). Stratigraphy and volcanic evolution of the middle Miocene to Pliocene La Grande–Owyhee eruptive axis in eastern Oregon. In S. P. Reidel, V. E. Camp, M. E. Ross, J. A. Wolff, B. S. Martin, T. L. Tolan, & R. E. Wells (Eds.), *The Columbia River flood basalt province*. Geological Society of America. https://doi.org/10.1130/2013.2497(16)

Ferns, M. L., McConnell, V. S., Madin, I. P., & Johnson, J. A. (2010). Geology of the Upper Grande Ronde River Basin, Union County, Oregon (DOGAMI Bulletin No. 107; p. 70).

Fitzgerald, J. F. (1982). Geology and Basalt Stratigraphy of the Weiser Embayment West-Central Idaho. In B. Bonnichsen & R. M. Breckenridge (Eds.), *Cenozoic Geology of Idaho: Idaho Bureau of Mines and Geology Bulletin* (Vol. 26, pp. 103–128).

Flowers, R. M., & Ehlers, T. A. (2018). Rock erodibility and the interpretation of low-temperature thermochronologic data. *Earth and Planetary Science Letters*, *482*, 312–323. https://doi.org/10.1016/j.epsl.2017.11.018

Flowers, R. M., Ketcham, R. A., Shuster, D. L., & Farley, K. A. (2009). Apatite (U-Th)/He thermochronometry using a radiation damage accumulation and annealing model. *Geochimica et Cosmochimica Acta*, *73*(8), 2347–2365. https://doi.org/10.1016/j.gca.2009.01.015

Flowers, R. M., Shuster, D. L., Farley, K. A., & Farley, K. A. (2007). Radiation damage control on apatite (U-Th)/He dates from the Grand Canyon region, Colorado Plateau. *Geology*, *5*, 447–450. https://doi.org/10.1130/G23471A.1

Foster, D. A., & Raza, A. (2002). Low-temperature thermochronological record of exhumation of the Bitterroot metamorphic core complex, northern Cordilleran Orogen. *Tectonophysics*, *349*(1–4), 23–36. https://doi.org/10.1016/S0040-1951(02)00044-6

Gallagher, K. (2012). Transdimensional inverse thermal history modeling for quantitative thermochronology. *Journal of Geophysical Research: Solid Earth*, *117*(B2). https://doi.org/10.1029/2011JB008825

Gaschnig, R. M., Macho, A. S., Fayon, A., Schmitz, M., Ware, B. D., Vervoort, J. D., et al. (2017). Intrusive and depositional constraints on the Cretaceous tectonic history of the southern Blue Mountains, eastern Oregon. *Lithosphere*, *9*(2), 265–282. https://doi.org/10.1130/L554.1

Gaschnig, R. M., Vervoort, J. D., Lewis, R. S., & McClelland, W. C. (2010). Migrating magmatism in the northern US Cordillera: In situ U–Pb geochronology of the Idaho batholith. *Contributions to Mineralogy and Petrology*, *159*(6), 863–883. https://doi.org/10.1007/s00410-009-0459-5

Gaschnig, R. M., Vervoort, J. D., Lewis, R. S., & Tikoff, B. (2011). Isotopic evolution of the Idaho batholith and Challis intrusive province, northern US Cordillera. *Journal of Petrology*, *52*(12), 2397–2429. https://doi.org/10.1093/petrology/egr050

Gautheron, C., Barbarand, J., Ketcham, R. A., Tassan-Got, L., van der Beek, P., Pagel, M., et al. (2013). Chemical influence on α-recoil damage annealing in apatite: Implications for (U–Th)/He dating. *Chemical Geology*, *351*, 257–267. https://doi.org/10.1016/j.chemgeo.2013.05.027

Giorgis, S., McClelland, W., Fayon, A., Singer, B. S., & Tikoff, B. (2008). Timing of deformation and exhumation in the western Idaho shear zone, McCall, Idaho. The *Geological Society of America Bulletin*, *120*(9–10), 1119–1133. https://doi.org/10.1130/B26291.1

Giorgis, S., Tikoff, B., Kelso, P., & Markley, M. (2006). The role of material anisotropy in the neotectonic extension of the western Idaho shear zone, McCall, Idaho. The *Geological Society of America Bulletin*, *118*(3–4), 259–273. https://doi.org/10.1130/B25382.1

Giorgis, S., Tikoff, B., & McClelland, W. (2005). Missing Idaho arc: Transpressional modification of the 87Sr/86Sr transition on the western edge of the Idaho batholith. *Geology*, *33*(6), 469. https://doi.org/10.1130/G20911.1

Guenthner, W. R., Reiners, P. W., Ketcham, R. A., Nasdala, L., & Giester, G. (2013). Helium diffusion in natural zircon: Radiation damage, anisotropy, and the interpretation of zircon (U-Th)/He thermochronology. *American Journal of Science*, *313*(3), 145–198. https://doi.org/10.2475/03.2013.01

Hales, T. C., Abt, D. L., Humphreys, E. D., & Roering, J. J. (2005). A lithospheric instability origin for Columbia River flood basalts and Wallowa Mountains uplift in northeast Oregon. *Nature*, *438*(7069), 842–845. https://doi.org/10.1038/nature04313

Hooper, P. R., Kleck, W. D., Knowles, C. R., Reidel, S. P., & Thiessen, R. L. (1984). Imnaha basalt, Columbia River basalt group. *Journal of Petrology*, *25*(2), 473–500. https://doi.org/10.1093/petrology/25.2.473

Janecke, S. U. (1994). Sedimentation and paleogeography of an Eocene to Oligocene rift zone, Idaho and Montana. The *Geological Society of America Bulletin*, *106*, 1083–1095. https://doi.org/10.1130/0016-7606(1994)106<1083:sapoae>2.3.co;2

Kahn, M., Fayon, A. K., & Tikoff, B. (2020). Constraints on the post-orogenic tectonic history along the Salmon River suture zone from low-temperature thermochronology, western Idaho and eastern Oregon. *Rocky Mountain Geology*, *55*(1), 27–54. https://doi.org/10.24872/rmgjournal.55.1.27

Karlstrom, L., Murray, K. E., & Reiners, P. W. (2019). Bayesian Markov-chain Monte Carlo inversion of low-temperature thermochronology around two 8 − 10 m wide Columbia River flood basalt dikes. *Frontiers of Earth Science*, *7*. https://doi.org/10.3389/feart.2019.00090

Kasbohm, J., & Schoene, B. (2018). Rapid eruption of the Columbia River flood basalt and correlation with the mid-Miocene climate optimum. *Science Advances*, *4*(9). https://doi.org/10.1126/sciadv.aat8223

LaMaskin, T. A., Vervoort, J. D., Dorsey, R. J., & Wright, J. E. (2011). Early Mesozoic paleogeography and tectonic evolution of the western United States: Insights from detrital zircon U-Pb geochronology, Blue Mountains Province, northeastern Oregon. The *Geological Society of America Bulletin*, *123*(9–10), 1939–1965. https://doi.org/10.1130/B30260.1

Lund, K., & Snee, L. W. (1988). Metamorphism, structural development and age of the continent-island juncture west-central Idaho. *Metamorphism and Crustal Evolution of the Western United States* (Vol. 7). Prentice-Hall.

McKay, M. P., Bollen, E. M., Gray, K. D., Stowell, H. H., & Schwartz, J. J. (2017). Prolonged metamorphism during long-lived terrane accretion: Sm-Nd garnet and U-Pb zircon geochronology and pressure-temperature paths from the Salmon River suture zone, west-central Idaho, USA. *Lithosphere*, *9*(5), 683–701. https://doi.org/10.1130/L642.1

Morriss, M. C., Karlstrom, L., Nasholds, M. W. M., & Wolff, J. A. (2020). The Chief Joseph dike swarm of the Columbia River flood basalts, and the legacy data set of William H. Taubeneck. *Geosphere*, *16*(4), 1082–1106. https://doi.org/10.1130/GES02173.1

Murray, K. E., Braun, J., & Reiners, P. W. (2018). Toward robust interpretation of low-temperature thermochronometers in magmatic terranes. *Geochemistry, Geophysics, Geosystems*, *19*(10), 3739–3763. https://doi.org/10.1029/2018GC007595

Murray, K. E., Reiners, P. W., Thomson, S. N., Robert, X., & Whipple, K. X. (2019). The thermochronologic record of erosion and magmatism in the Canyonlands region of the Colorado Plateau. *American Journal of Science*, *319*(5), 339–380. https://doi.org/10.2475/05.2019.01

Orme, D. O., Guenthner, W. R., Laskowski, A. K., & Reiners, P. W. (2016). Long-term tectonothermal history of Laramide basement from zircon–He age-eU correlations. *Earth and Planetary Sciences Letters 453*, 119–130.

Petcovic, H. L., & Dufek, J. D. (2005). Modeling magma flow and cooling in dikes: Implications for emplacement of Columbia River flood basalts. *Journal of Geophysical Research*, *110*(B10). https://doi.org/10.1029/2004JB003432

Petcovic, H. L., & Grunder, A. L. (2003). Textural and thermal history of partial melting in Tonalitic Wallrock at the margin of a basalt dike, Wallowa mountains, Oregon. *Journal of Petrology*, *44*(12), 2287–2312. https://doi.org/10.1093/petrology/egg078

Reidel, S. P., Camp, V. E., Tolan, T. L., Kauffman, J. D., & Garwood, D. L. (2013). Tectonic evolution of the Columbia River flood basalt province. *Columbia River Flood Basalt Province* (Vol. 497). Geological Society of America. Retrieved from https://pubs.geoscienceworld.orghttps://pubs.geoscienceworld.org/books/book/661/chapter/3807278/Tectonic-evolution-of-the-Columbia-River-flood

Reidel, S. P., Tolan, T. L., Hooper, P. R., Beeson, M. H., Fecht, K. R., Bentley, R. D., & Anderson, J. L. (1989). The Grande Ronde basalt, Columbia River basalt group; stratigraphic descriptions and correlations in Washington, Oregon, and Idaho. *Geological Society of America Special Papers* (Vol. 239, pp. 21–54). Geological Society of America. https://doi.org/10.1130/SPE239-p21

Reiners, P. W. (2003). Post-orogenic evolution of the Dabie Shan, eastern China, from (U-Th)/He and fission-track thermochronology. *American Journal of Science*, *303*(6), 489–518. https://doi.org/10.2475/ajs.303.6.489

Reiners, P. W. (2005a). (U-Th)/(He-Pb) double dating of detrital zircons. *American Journal of Science*, *305*(4), 259–311. https://doi.org/10.2475/ajs.305.4.259

Reiners, P. W. (2005b). Zircon (U-Th)/He thermochronometry. *Reviews in Mineralogy and Geochemistry*, *58*(1), 151–179. https://doi.org/10.2138/rmg.2005.58.6

Reiners, P. W. (2007). Thermochronologic approaches to paleotopography. *Reviews in Mineralogy and Geochemistry*, *66*(1), 243–267. https://doi.org/10.2138/rmg.2007.66.10

Retallack, G. J., Bestland, E. A., & Fremd, T. J. (2000). *Eocene and Oligocene Paleosols of central Oregon* (p. 344). Geological Society Special Publications.

Rogers, J. (1966). Coincidence of structural and topographic highs during post-Clarno time in north-central Oregon: Geological notes. *AAPG Bulletin*, *50*. https://doi.org/10.1306/5D25B497-16C1-11D7-8645000102C1865D

Schildgen, T. F., van der Beek, P. A., Sinclair, H. D., & Thiede, R. C. (2018). Spatial correlation bias in late-Cenozoic erosion histories derived from thermochronology. *Nature*, *559*(7712), 89–93. https://doi.org/10.1038/s41586-018-0260-6

Schmidt, K. L., Lewis, R. S., Vervoort, J. D., Stetson-Lee, T. A., Michels, Z. D., & Tikoff, B. (2017). Tectonic evolution of the Syringa embayment in the central North American Cordilleran accretionary boundary. *Lithosphere*, *9*(2), 184–204. https://doi.org/10.1130/L545.1

Schoettle-Greene, P., Duvall, A. R., Blythe, A., Morley, E., Matthews, W., & LaHusen, S. R. (2020). Uplift and exhumation in Haida Gwaii driven by terrane translation and transpression along the southern Queen Charlotte fault, Canada. *Geology*, *48*(9), 908–912. https://doi.org/10.1130/G47364.1

Schwartz, J. J., Johnson, K., Mueller, P., Valley, J., Strickland, A., & Wooden, J. L. (2014). Time scales and processes of Cordilleran batholith construction and high-Sr/Y magmatic pulses: Evidence from the Bald Mountain batholith, northeastern Oregon. *Geosphere*, *10*(6), 1456–1481. https://doi.org/10.1130/GES01033.1

Schwartz, J. J., Snoke, A. W., Cordey, F., Johnson, K., Frost, C. D., Barnes, C. G., et al. (2011). Late Jurassic magmatism, metamorphism, and deformation in the blue mountains province, northeast Oregon. The *Geological Society of America Bulletin*, *123*(9–10), 2083–2111. https://doi.org/10.1130/B30327.1

Schwartz, J. J., Snoke, A. W., Frost, C. D., Barnes, C. G., Gromet, L. P., & Johnson, K. (2010). Analysis of the Wallowa-Baker terrane boundary: Implications for tectonic accretion in the Blue Mountains province, northeastern Oregon. *GSA Bulletin*, *122*(3–4), 517–536. https://doi.org/10.1130/B26493.1

Seligman, A. N., Bindeman, I. N., McClaughry, J., Stern, R. A., & Fisher, C. (2014). The earliest low and high 18O caldera-forming eruptions of the Yellowstone plume: Implications for the 30-40 Ma Oregon calderas and speculations on plume-triggered delaminations. *Frontiers of Earth Science*, *2*. 1–9. https://doi.org/10.3389/feart.2014.00034

Shuster, D. L. & Farley, K. A. (2009). The influence of artificial radiation damage and thermal annealing on helium diffusion kinetics in apatite. *Geochimica et Cosmochimica Acta 73*, 183–196.

Swanson, D. A., Anderson, J. L., Camp, V. E., Hooper, P. R., Taubeneck, W. H., & Wright, T. L. (1981). *Reconnaissance geologic map of the Columbia River basalt group, northern Oregon and western Idaho [Map]*. USGS.

Sweetkind, D. S., & Blackwell, D. D. (1989). Fission-track evidence of the Cenozoic thermal history of the Idaho batholith. *Tectonophysics*, *157*(4), 241–250. https://doi.org/10.1016/0040-1951(89)90142-X

Tikoff, B., Kelso, P., Manduca, C., Markley, M. J., & Gillaspy, J. (2001). Lithospheric and crustal reactivation of an ancient plate boundary: The assembly and disassembly of the Salmon River suture zone, Idaho, USA. *Geological Society, London, Special Publications*, *186*(1), 213–231. https://doi.org/10.1144/GSL.SP.2001.186.01.13

VanTassell, J., Ferns, M., McConnell, V., & Smith, G. R. (2001). The mid-Pliocene Imbler fish fossils, Grande Ronde valley, union County, Oregon, and the connection between lake Idaho and the Columbia River. *Oregon Geology*, *63*(3).

Wells, R. E., Bukry, D., Friedman, R., Pyle, D., Duncan, R., Haeussler, P., & Wooden, J. (2014). Geologic history of Siletzia, a large igneous province in the Oregon and Washington Coast Range: Correlation to the geomagnetic polarity time scale and implications for a long-lived Yellowstone hotspot. *Geosphere*, *10*(4), 692–719. https://doi.org/10.1130/GES01018.1

Willett, S. D., & Brandon, M. T. (2002). On Steady States in Mountain Belts. *Geology*, *30*(2), 175.

Wolf, R. A., Farley, K. A., & Kass, D. M. (1998). Modeling of the temperature sensitivity of the apatite U–Th/He thermochronometer. *Chemical Geology*, *148*, 105–114.

Wolfe, J. A. (1992). An analysis of present-day terrestrial lapse rates in the western Conterminous United States and their significance to Paleoaltitudianal estimates. USGS Bulletin No. 1962.

Žák, J., Verner, K., Tomek, F., Holub, F. V., Johnson, K., & Schwartz, J. J. (2015). Simultaneous batholith emplacement, terrane/continent collision, and oroclinal bending in the Blue Mountains Province, North American Cordillera. *Tectonics*, *34*(6), 1107–1128. https://doi.org/10.1002/2015TC003859

Zapata, S., Sobel, E. R., del Papa, C., Jelinek, A. R., & Glodny, J. (2019). Using a paleosurface to constrain low-temperature thermochronological data: Tectonic evolution of the Cuevas range, central Andes. *Tectonics*, *38*(11), 3939–3958. https://doi.org/10.1029/2019TC005887

References From the Supporting Information

Farley, K. A., Wolf, R. A., & Silver, L. T. (1996). The effects of long alpha-stopping distances on (U-Th)/He ages. *Geochimica et Cosmochimica Acta*, *60*(21), 4223–4229. https://doi.org/10.1016/S0016-7037(96)00193-7

Johnson, K. J. J., Schwartz, J. J., Wooden, J. L., O'Driscoll, L. J., & Jeffcoat, R. C. (2011). The Wallowa batholith: New Pb/U (SHRIMP–RG) ages place constraints on arc magmatism and crustal thickening in the Blue Mountains Province, NE Oregon [Abstracts with Programs]. *Geological Society of America*, *43*, 5.

Ketcham, R. A., Gautheron, C., & Tassan-Got, L. (2011). Accounting for long alpha-particle stopping distances in (U–Th–Sm)/He geochronology: Refinement of the baseline case. *Geochimica et Cosmochimica Acta*, *75*(24), 7779–7791. https://doi.org/10.1016/j.gca.2011.10.011

Mitchell, S. G., & Reiners, P. W. (2003). Influence of wildfires on apatite and zircon (U-Th)/He ages. *Geology*, *31*(12), 1025–1028. https://doi.org/10.1130/G19758.1

Ross, S. M. (2003). Peirce's criterion for the elimination of suspect experimental data. *Journal of Engineering Technology*, *12*.